LITHOS 488–489 (2024) 107783

Contents lists available at ScienceDirect

LITHOS

journal homepage: www.elsevier.com/locate/lithos

Diffusion-induced stress in crystals: Implications for timescales of mountain building

Benjamin L. Hess [a,*], Jay J. Ague [a,b]

[a] Department of Earth and Planetary Sciences, Yale University, PO Box 208109, New Haven, CT 06520-8109, USA
[b] Yale Peabody Museum of Natural History, Yale University, New Haven, CT 06511, USA

ARTICLE INFO

Keywords:
Garnet
Diffusion chronometry
Non-hydrostatic stress
Mountain building
Regional metamorphism
Glen Clova, Scotland

ABSTRACT

Intracrystalline chemical diffusion offers valuable insights into the durations of metamorphic and igneous processes. However, it can yield timescale estimates for orogenic and subduction zone events that are considerably shorter than those obtained via isotopic geochronology. One potential explanation that has been offered for the discrepancy is that the interdiffusion of species with different atomic or ionic radii may generate intracrystalline, compositional stresses that alter or limit diffusional relaxation. In this study we test this idea by developing and applying the compositional stress theory of materials scientists F. Larché and J. Cahn to garnet from the Barrovian sillimanite zone, Scotland. Relaxed contacts from the garnet, independent diffusion chronometers, and thermal modeling all indicate a >100 kyr duration for peak temperature metamorphism. Nonetheless, the garnet records sharp, μm-scale variations in calcium and iron contents that standard diffusion treatments predict should relax in 1–10 kyr at peak temperature conditions. Our results show that the development of compositional stress during diffusional relaxation can explain the preservation of the observed short wavelength compositional oscillations at a >100 kyr timescale. Thus, it may be necessary to account for compositional stress when modeling diffusion in solid solutions with appreciable differences in their endmember molar volumes. This will be particularly relevant when considering sharp, μm-scale chemical gradients involving grossular, the garnet endmember with the largest molar volume relative to pyrope, almandine, and spessartine. Neglecting compositional stress in such cases could result in the underestimation of the timescales of lithospheric processes by potentially orders of magnitude. The effects of compositional stress in garnet are predicted to be the most pronounced under amphibolite and blueschist–eclogite facies conditions. At lower temperatures diffusion is limited, and at higher temperatures both plastic deformation and more ideal solid solution behavior will act to diminish the impact of stress.

1. Introduction

The extent of intracrystalline chemical diffusion between minerals or between distinct compositional zones within minerals offers a powerful chronometer for estimating the timescales of metamorphic and igneous processes (e.g., Ague and Carlson, 2013; Ganguly, 2010; Kohn and Penniston-Dorland, 2017; Lasaga, 1983; Spear, 1991; Watson and Baxter, 2007). Such diffusion chronometry has provided valuable and unique constraints on rates of heating, magmatism, fault movement, fluid infiltration, retrograde cooling, and exhumation (e.g., Ague and Baxter, 2007; Chen and Chu, 2024; Chu et al., 2017; Devoir et al., 2021; Dragovic et al., 2016; Erambert and Austrheim, 1993; Faryad and Chakraborty, 2005; Florence and Spear, 1995; Gaidies et al., 2021; Perchuk et al., 1999; Schwarzenbach et al., 2021; Spear et al., 2012; Viete and Lister, 2017).

However, diverse tectonometamorphic studies have revealed provocative discrepancies between timescales obtained by diffusion chronometry compared to isotopic geochronology, particularly in regional metamorphic and subduction zone settings. For example, diffusion chronometry can indicate $<10^3$-to-10^5-year timescales compared to the 10^6-to-10^7-year timescales obtained from geochronology for the same tectonic event (Viete and Lister, 2017). In some cases, these disparate results reflect transient heat and/or mass transfer episodes spread out over the duration of an orogeny; for example, pulses of fluids, magmas,

* Corresponding author.
E-mail address: benjamin.hess@yale.edu (B.L. Hess).

https://doi.org/10.1016/j.lithos.2024.107783
Received 12 June 2024; Received in revised form 26 August 2024; Accepted 28 August 2024
Available online 2 September 2024

or shear heating (e.g., Ague and Baxter, 2007; Chu et al., 2017; Erambert and Austrheim, 1993; Viete and Lister, 2017). Nonetheless, the enormous range of timescale estimates demands further interrogation.

Another possibility is that chemical diffusion-based methods may underestimate timescales in some situations due to factors such as intracrystalline stress. There has long been recognition of the mutual interactions of stress and diffusion (e.g., Herring, 1950; Zener, 1948). For example, the Gorsky effect posits that stress fields will cause chemical species to diffuse as a function of their relative molar volumes to reduce strain energy (Gorsky, 1935; Hess and Ague, 2023; Shi et al., 2018). Furthermore, it has been proposed that interdiffusion of different-sized species can strain a crystal's lattice, generating stresses in an initially stress-free crystal (Larché and Cahn, 1982). It has been suggested that such diffusion-induced stresses within crystals could slow or prevent the relaxation of compositional features, affecting diffusion chronometry methods (e.g., Baumgartner et al., 2010; Larché and Cahn, 1982, 1985; Tajčmanová et al., 2014, 2015; Viete and Lister, 2017; Zhong et al., 2017).

Nonetheless, this idea remains largely untested as standard diffusion models implicitly assume a constant pressure, and therefore, the impact of stress on diffusion remains uncertain. To overcome this problem, methods are required to both quantify diffusion-induced stresses and treat their impact on the chemical evolution of minerals. Herein, we combine the theoretical framework of Larché and Cahn (1982, 1985) with recent treatments of multicomponent solid solution (Hess et al., 2022) and diffusion (Hess and Ague, 2023) to model the coupling of stress and diffusion in almandine–pyrope–grossular–spessartine (Alm–Py–Grs–Sps) quaternary garnet. There is yet no example of which we are aware that demonstrates quantitative agreement between observed multicomponent chemical element zonation (natural or experimental) and compositional stress theory. Without further testing, we cannot determine the potential impact of compositional stress on intracrystalline diffusion and the evolution of crystal chemistry.

We test compositional stress theory by applying our treatment to garnet from Glen Clova, Scotland. As the type-locality for Barrovian metamorphism, samples from this locality are well characterized in terms of pressure, temperature, and time history (e.g., Ague et al., 2001; Ague and Baxter, 2007; Barrow, 1893; Baxter et al., 2002; McLellan, 1985; Viete and Lister, 2017; Vorhies and Ague, 2011). The timescale of peak temperature metamorphism, between 100 and 400 kyr, has been independently constrained by Sr-in-apatite diffusion chronometry, garnet diffusion chronometry, and thermal conduction modeling (Ague and Baxter, 2007; Chu and Ague, 2015; Viete and Lister, 2017).

However, new high resolution chemical profiles presented in this study reveal micrometer-scale composition oscillations that suggest peak thermal timescales of 1–10 kyr—far shorter than the independently constrained 100–400 kyr. Here we posit that compositional stress could explain the preservation of these short-wavelength features at >100 kyr timescales, consistent with the independent timescale estimates. The essential finding is that the large size of grossular compared to the other endmembers generates compositional stress during diffusion that prevents the relaxation of the small-scale, sharp chemical features, allowing them to persist for longer timescales than predicted by standard diffusion models. Thus, garnets with variations in grossular may develop intracrystalline compositional stresses that could potentially change the timescales interpreted from garnet diffusion chronometry by orders of magnitude.

2. Methods

2.1. Electron probe microanalysis (EPMA)

Quantitative chemical profiles were collected using the JEOL JXA-8530F field-emission gun EPMA at Yale University, employing a focused beam, 100 nA beam current, 10 kV accelerating voltage, wavelength-dispersive spectrometers, linear off-peak background corrections, natural and synthetic standards, $\phi(\rho z)$ matrix corrections, and a 1 μm step size. The 10 kV accelerating voltage decreases the activation volume of garnet to approximately 1–1.5 μm, thus providing higher spatial resolution for the chemical profiles (Fig. S1; Ague and Eckert Jr., 2012). Uncertainties on plotted mole fractions are $\pm 2\sigma$ sample standard deviations (SDs) based on the measured Poisson counting statistics for each element. Maps were collected at 300 nA and 15 kV using wavelength-dispersive spectrometers and grid spacings of either 1.3 or 5 μm. The edges of Profiles 3 and 4 (below) were quantitatively extended using x-ray counts from the chemical maps to demonstrate that the compositions are relatively flat well beyond the high-variability regions mapped in detail with 1-μm resolution (see Supplementary Material). This can also be qualitatively ascertained just by inspection of the maps.

2.2. Profile fit statistics

An *F*-test for equality of variances was used to compare the grossular and almandine mole fraction residuals between the best fits with and without compositional stress. In the following, the mean is defined as the arithmetic mean of the grossular and almandine residuals in a profile, and the SD is the standard deviation of the grossular and almandine residuals. The residuals are defined as the difference between the mole fraction values of the model result and the observed values.

For Profile 4 the data points from $r = 30$ μm to 60 μm were used as they capture the width of the relaxed contact. The residuals had mean = 0.000146, SD = 0.00189 with compositional stress and mean = 0.000218, SD = 0.00234 without compositional stress. The standard deviations of the residuals were not statistically different ($p = 0.26$).

For the remaining profiles, the 1 μm spaced data points were used. For Profile 1 the parameters for the best fits were $N = 147$, mean = −0.000103, and SD = 0.00174 with compositional stress and $N = 147$, mean = −0.000101, and SD = 0.00326 without compositional stress. For Profile 3 the parameters for the best fits were $N = 121$, mean = 0.000213, and SD = 0.00151 with compositional stress and $N = 121$, mean = 0.000213, and SD = 0.00257 without compositional stress. Finally, for Profile 6 the parameters for the best fits were $N = 142$, mean = −0.000109, and SD = 0.00221 with compositional stress and $N = 142$, mean = −0.000084, and SD = 0.00391 without compositional stress. The SDs of the residuals are different at a statistical significance level of $p < 1 \times 10^{-7}$ for Profiles 1, 3, and 6.

3. Theory and calculations

3.1. Diffusion and Larché-Cahn theory

Intracrystalline diffusion follows Fick's law such that the flux of a species in a solid is linearly proportional to its Gibbsian chemical potential gradient. At a constant pressure and temperature, the chemical potentials in a multicomponent solid are a function of only the composition, and thus, it is standard practice to use concentration or mole fraction gradients to model diffusion (e.g., Borinski et al., 2012).

This simplification cannot be made when treating the impact of stress on diffusion. Incorporating stress requires using Fick's Law with the underlying free energy gradients, as pressure is no longer constant. However, chemical potential is insufficient to treat gradients in stress as it is defined only for constant pressure. If there are gradients in intracrystalline stress, chemical potential cannot be used to meaningfully define the free energy of a solid (Hess and Ague, 2023; Hess et al., 2022; Larché and Cahn, 1985; Wheeler, 2018).

The work of materials scientists Larché and Cahn (1982, 1985), or Larché-Cahn theory, provides a means to overcome this problem and treat the effects of stress on solid thermodynamics and kinetics. Hailed as a "milestone of 20th century thermodynamics" (Shi et al., 2018), Larché-Cahn theory is well-established and has been widely applied (Clavijo et al., 2022; Cui et al., 2012; Erdélyi and Schmitz, 2012; Gurtin

et al., 2010; Hess and Ague, 2021, 2023; Hess et al., 2022; Powell et al., 2018; Shi et al., 2018; Stephenson, 1988; Tomozawa and Davis, 1999; Voorhees and Johnson, 2004; Wheeler, 2018).

Larché-Cahn theory recognizes that the chemical equilibrium of multicomponent crystals is achieved when no molar exchanges of species on lattice sites can lower the overall energy of a crystal. Quantifying the energy change in a crystal due to the exchange of species gives rise to a thermodynamic potential called the diffusion potential (or relative chemical potential; Gurtin et al., 2010) that describes the energy change due to the stoichiometric exchange of species on lattice sites. Larché and Cahn (1985) show that even if the chemical potential cannot be defined for the interiors of stressed solids, the energetic difference between chemical species can be. Thus, relative chemical potential gradients provide the driving force that allows for diffusion to be modeled in stressed crystals (Cahn and Larché, 1983; Hess and Ague, 2023; Larché and Cahn, 1982, 1985). Hess and Ague (2023) provide a diffusion treatment based on relative chemical potential which we use here to explore the impact of stress on diffusion (Section 3.2.).

Larché and Cahn (1982) also provide a method for calculating diffusion-induced "self-stress" (i.e., stress caused by changes in composition relative to a reference state) and incorporating its effect on the evolution of chemical zonation. Diffusion between species of different sizes in a crystalline solid is expected to cause the structure to expand or contract locally. However, the geometric constraints and mechanical properties of the crystal lattice can impede or prevent these local volume changes from occurring. As a result, the crystal becomes strained (and thus, stressed) relative to its pre-diffusion state (Voorhees and Johnson, 2004). We refer to this "self-stress" as compositional stress, indicating stress caused by composition change. Chemical diffusion and thermal conduction follow the same general governing equations. Consequently, Larché and Cahn (1982) recognized that compositional stresses caused by lattice expansions or contractions due to chemical diffusion are analogous to thermal stresses caused by expansions or contractions due to thermal conduction. Therefore, well-known thermoelasticity equations can be modified to quantify compositional stress (Section 3.3.).

3.2. Diffusion flux expression

We employ a multicomponent flux expression derived using gradients in relative chemical potential (Hess and Ague, 2023):

$$J_I^X = -u_I X_I \frac{\partial \mu_{I-N}}{\partial x} + u_I X_I z_I \frac{\sum_{K=1}^{N-1}\left(u_K X_K z_K \frac{\partial \mu_{K-N}}{\partial x}\right)}{\sum_{J=1}^{N}\left(u_J X_J z_J^2\right)} \tag{1}$$

where J_I^X is the mole fraction flux of endmember I (moles of I per total moles $m^{-2}\ s^{-1}$), u_I is the mobility of constituent I (m^2 mol $J^{-1}\ s^{-1}$), X_I is the mole fraction of constituent I (unitless), μ_{I-N} is the relative chemical potential per m^3 between independent constituent I and dependent constituent N (J mol^{-1}), and z_I is the charge number for I (unitless). The full derivation for eq. (1) is found in Hess and Ague (2023). The choice of the N^{th}, dependent endmember is arbitrary and does not affect the results.

Mobility is calculated from the well-known Nernst-Einstein equation (e.g., Cahn and Larché, 1983):

$$u_I = \frac{D_I}{RT} \tag{2}$$

where D_I is the self-diffusion coefficient ($m^2\ s^{-1}$), R is the ideal gas constant (J $mol^{-1}\ K^{-1}$), and T is the absolute temperature (K).

The flux can then be re-written as a linear sum of mobility-based interdiffusion coefficients, B_{IJ}, and relative chemical potential gradients (Eq. (8.1) of Larché and Cahn, 1985):

$$J_I^X = -\sum_{J=1}^{N-1} B_{IJ} \frac{\partial \mu_{J-N}}{\partial x} \tag{3}$$

in which

$$B_{IJ} = u_I X_I \delta_{IJ} - u_I X_I z_I \frac{u_J X_J z_J}{\sum_{K=1}^{N} u_K X_K z_K^2} \tag{4}$$

where δ_{IJ} is the Kronecker delta. The matrix B_{IJ} represents the Onsager transport coefficients, linking the $N-1$ independent relative chemical potential gradients which drive diffusion to the flux of the $N-1$ independent diffusing components. As the matrix is symmetric, it upholds the fundamental Onsager reciprocal relations (Hess and Ague, 2023).

The relative chemical potential is calculated assuming that garnet is structurally isotropic and its elastic parameters do not change significantly with composition (Larché and Cahn, 1985; Erba et al., 2014; Hess et al., 2022; Hess and Ague, 2023):

$$\mu_{I-N}(\sigma_m, T) = \mu_I(P, T) - \mu_N(P, T) - 3V_0\Omega^{I-N}(\sigma_m + P) \tag{5}$$

where $\mu_{I-N}(\sigma_m, T)$ is the relative chemical potential (J mol^{-1}) between constituents I and N at a given mean stress (σ_m; Pa) and temperature (K); $\mu_I(P, T)$ and $\mu_N(P, T)$ are the chemical potentials of I and N (J mol^{-1}) at the given reference pressure and temperature; V_0 is the molar volume of the solid (i.e., the sum of the endmember partial molar volumes) in the reference state ($m^3\ mol^{-1}$); and Ω^{I-N} is the partial molar strain between I and N (unitless). Partial molar strain represents the lattice strain due to composition change and is a scalar value for isotropic and cubic materials (Larché and Cahn, 1985; Voorhees and Johnson, 2004; Wheeler, 2018). The mean stress is defined as the average of the diagonal components of the stress tensor which encompasses the reference pressure and compositional stress (see below). The thermodynamic database of Holland and Powell (2011) and activity model of White et al. (2014) are used for garnet. Garnet is mechanically anisotropic, but its anisotropy is low (Erba et al., 2014) and therefore the elastic constants can be treated as isotropic to first order (Hess and Ague, 2023; Hess et al., 2022; Wheeler, 2018).

3.3. Compositional stress

We calculate multicomponent compositional stress following Larché and Cahn (1982) with linear viscous relaxation following Stephenson (1988) and Erdélyi and Schmitz (2012). The necessary information to derive the following equations is given on p. 1809–1810 of Erdélyi and Schmitz (2012) with details given in the Supplementary Material.

Compositional stress in a solid sphere with a constant pressure boundary condition is given by:

$$\sigma_{rr} = \frac{2E}{1-\nu}\left(\frac{1}{R_o^3}\int_0^{R_o} r^2\left[\varepsilon^{SF} + \frac{1-2\nu}{1+\nu}\left(\varepsilon_{rr}^p + A\right)\right]dr - \frac{1}{r^3}\int_0^{r} r^2\left[\varepsilon^{SF} + \frac{1-2\nu}{1+\nu}\left(\varepsilon_{rr}^p + A\right)\right]dr\right) + \frac{E}{1+\nu}\left(A - A(R_o)\right) - P \tag{6}$$

and

$$\sigma_{\theta\theta} = \sigma_{\phi\phi} = \frac{E}{1-\nu}\left(\frac{2}{R_o^3}\int_0^{R_o} r^2\left[\varepsilon^{SF} + \frac{1-2\nu}{1+\nu}\left(\varepsilon_{rr}^p + A\right)\right]dr + \frac{1}{r^3}\int_0^{r} r^2\left[\varepsilon^{SF} + \frac{1-2\nu}{1+\nu}\left(\varepsilon_{rr}^p + A\right)\right]dr\right) - \frac{E}{1-\nu}\left(\varepsilon^{SF} - \frac{\varepsilon_{rr}^p}{2} - \frac{\nu}{1+\nu}A + A(R_o)\right) - P \tag{7}$$

where

$$A = 3\int_0^r \frac{\varepsilon_{rr}^p}{r} dr \tag{8}$$

Here, σ_{rr} is the radial stress (Pa), $\sigma_{\theta\theta}$ and $\sigma_{\phi\phi}$ are the tangential stresses (Pa), E is the Young's modulus (Pa), ν is Poisson's ratio (unitless), R_o is the outer radius of the sphere (m), r is the radius (m), ε^{SF} is the stress-free strain (unitless), ε_{rr}^p is the radial plastic strain (unitless), and P is the reference pressure (Pa). By convention, pressure is positive and compressive stress is negative, hence pressure is subtracted (Larché and Cahn, 1985). We use constant values of 240 GPa and 0.27 for the Young's modulus (E) and Poisson's ratio (ν), respectively, for garnet (Erba et al., 2014; Hess and Ague, 2023).

The stress-free strain is the strain resulting from composition change relative to the reference state which is taken to be the initial condition in our models (i.e., the initial pressure, temperature, and composition). Stress-free strain is a scalar value in this case because we treat garnet as isotropic, and it is given by the sum of the partial molar strain multiplied by the composition change for each independent endmember pair, X_{I-N}, relative to the initial composition:

$$\varepsilon^{SF} = \sum_{I=1}^{N-1} \Omega^{I-N} \Delta X_{I-N} \tag{9}$$

For isotropic and cubic materials, $\Omega^{I-N} = \frac{V_I - V_N}{3V_0}$ where V_I and V_N are the molar volumes of I and N, respectively (Larché and Cahn, 1985). Taking Grs to be the dependent endmember and using Holland and Powell (2011) to calculate garnet endmember molar volumes, the partial molar strains for this garnet at 0.6 GPa and 660 °C are approximately $\Omega^{\mathrm{Alm-Grs}} = -0.0295$, $\Omega^{\mathrm{Py-Grs}} = -0.0348$, and $\Omega^{\mathrm{Sps-Grs}} = -0.0215$. The negative values indicate that the lattice size decreases as Grs is replaced by other endmembers. Since molar volumes are relatively insensitive to temperature and pressure changes, the partial molar strain values do not vary appreciably with changing conditions.

An additional term can be added to Eq. (9) to account for vacancy creation and destruction (Erdélyi and Schmitz, 2012; Stephenson, 1988); however, we assume that lattice sites are conserved. This is reasonable given the absence of any observed interface migration (i.e., the Kirkendall effect). Finally, the radial plastic strain, ε_{rr}^p is given by integrating the following with respect to time (Eq. (42) in Erdélyi and Schmitz, 2012):

$$\dot{\varepsilon}_{rr}^p = \frac{1}{3\eta}(\sigma_{rr} - \sigma_{\theta\theta}) \tag{10}$$

where $\dot{\varepsilon}_{rr}^p$ is the instantaneous strain rate and η is the viscosity (10^{24} Pa·s is used for garnet in this study; Wang and Ji, 1999).

The equations for a planar geometry are analogous (see appendix A in Erdélyi and Schmitz, 2012):

$$\sigma_{xx} = -P \tag{11}$$

and

$$\sigma_{yy} = \sigma_{zz} = -\frac{E}{1-\nu}\left(\varepsilon^{SF} - \frac{\varepsilon_{xx}^p}{2}\right) - P \tag{12}$$

where σ_{xx}, σ_{yy}, and σ_{zz} are the stresses in the x, y, and z directions (Pa), respectively, ε_{xx}^p is the plastic strain in the x direction (unitless), and all other terms are as previously defined. The stress-free strain, ε^{SF}, is the same as in the spherical case (Eq. (12)). Integrating the following equation with respect to time yields the plastic strain:

$$\dot{\varepsilon}_{xx}^p = -\frac{1}{3\eta}\sigma_{yy} \tag{13}$$

The mean stress, σ_m, is then calculated as follows. For the spherical case: $\sigma_m = \frac{\sigma_{rr}+\sigma_{\theta\theta}+\sigma_{\phi\phi}}{3}$, and for the planar case: $\sigma_m = \frac{\sigma_{xx}+\sigma_{yy}+\sigma_{zz}}{3}$. If the solid is assumed to be perfectly elastic, Eqs. (6)–(13) reduce to the equations given in Larché and Cahn (1982).

3.4. Numerical algorithm

First, the relative chemical potentials for garnet endmembers at each point are calculated at the given ambient pressure and temperature of the system using eq. (5) along with the thermodynamic database of Holland and Powell (2011) and activity model of White et al. (2014). Likewise, the self-diffusion coefficients are calculated at each point using the calibration of Chu and Ague (2015) with Mn coefficients from Chen and Chu (2024) and an oxygen fugacity of $10^{-18.25}$ bars for the sample under consideration (Ague et al., 2001).

Having defined the initial condition and variables, diffusion is modeled by iterating the following procedure with zero flux boundary conditions (i.e., the garnet does not exchange cations with the matrix):

1. The 1D mole fraction flux is calculated using either a spherical or planar forward time centered space (FTCS) method (e.g., Roache, 1972) to solve Eq. (3) at each point using a distance spacing of 0.2 μm and time step of 0.5–2 yr, depending on the profile.
2. The compositional stress and viscous relaxation at each point are then numerically calculated using either Eqs. (6)–(10) for a spherical geometry or Eqs. (11)–(13) for a planar geometry.
3. The relative chemical potentials and interdiffusion coefficients are re-computed using Eqs. (5) and (4), respectively.

3.5. Convolution correction

Although the beam from electron microprobe analysis can be focused to a spot size of approximately 100 nm, the beam excites a larger region with a diameter of approximately 1–1.5 μm (e.g., Ganguly et al., 1988; Ague and Eckert Jr., 2012; Chen and Chu, 2024). Thus, the measured data are convolved and represent a spatial average composition over the excited volume for each measurement. This means chemical contacts will appear to be smoother in the observed data than they actually are (Fig. S1a). This smoothing can be exacerbated if the chemical contact is tilted (Fig. S1b). To account for convolution, we apply a convolution correction to our model results following the methodology given by Ganguly et al. (1988) using a convolution factor of 0.48 (Borinski et al., 2012).

4. Results

We first present a theoretical example of the effects of compositional stress on diffusion in a hypothetical Alm–Py–Grs–Sps garnet and then turn to a natural example from Glen Clova, Scotland.

4.1. Theoretical example: model setup

We model radial multicomponent diffusion in a hypothetical garnet. The Al-Si-O framework of garnet is treated as a static network which allows Fe^{2+}, Mg^{2+}, Ca^{2+}, and Mn^{2+} to diffuse between discrete dodecahedral sites. Endmember relative chemical potential gradients are then defined by the energy change caused by the exchange of these ions (Hess and Ague, 2023). The model garnet has initial step function variations in X_{Grs} and X_{Alm} and uniform X_{Py} and X_{Sps} (X denotes mole fraction). We compare the model results with and without compositional stress (Figs. 1 and S2).

In our compositional stress model, we assume that the garnet is initially stress-free (i.e., initially at a uniform pressure), meaning that each compositional zone grew such that there were no initial deviations from its expected molar volume at the given pressure and temperature conditions. It is only after the mineral has grown, fixing the geometry and crystal lattice, that subsequent diffusional composition change will

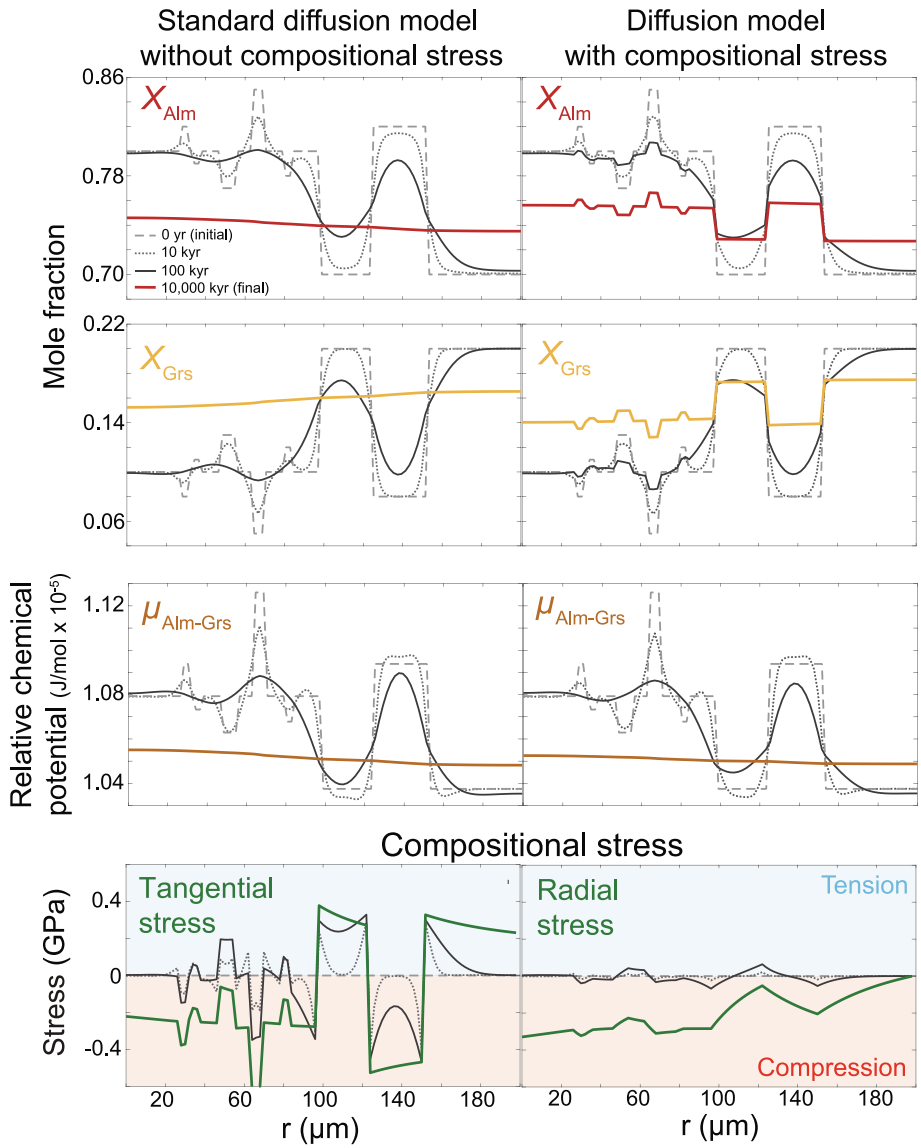

Fig. 1. Modeled diffusional relaxation of a hypothetical spherical garnet profile at 700 °C and 1 GPa with and without compositional stress. The garnet has initial step variations in X_{Grs} and X_{Alm}, uniform X_{Py} and X_{Sps}, and is initially at a uniform pressure. The top three rows show the modeled profiles for X_{Grs}, X_{Alm}, and relative chemical potential between Alm and Grs ($\mu_{Alm-Grs}$) with and without compositional stress. Note that at the end of the simulations, sharp oscillations in X_{Grs} and X_{Alm} remain in the compositional stress model but are fully smoothed in the standard model. The bottom row shows the modeled compositional stress arising from diffusion. Perfectly elastic behavior is assumed as it clearly illustrates the influence of compositional stress. The evolution of X_{Py}, X_{Sps}, μ_{Py-Grs}, and $\mu_{Sps-Grs}$ are shown in Fig. S2.

generate compositional stresses. We note that there will be a degree of lattice mismatch at the contacts between different compositional zones during growth which may generate nanometer-scale stresses and strains. However, these extremely localized effects would not appreciably influence the chemical evolution of the garnet (Fig. S3).

We treat the garnet rim as a free surface at constant pressure that is allowed to expand and contract. Compressional stress is defined as negative and extensional stress as positive by convention. We further assume that there is no viscous relaxation (i.e., infinite viscosity) in this first example to isolate and thus clearly show the impact of compositional stress on the evolution of chemical profiles. The magnitude of compositional stress is a function of endmember molar volume differences and elastic parameters. These values are reasonably well-constrained and relatively insensitive to changes in temperature and pressure at crustal conditions (Erba et al., 2014; Holland and Powell, 2011). Given the large magnitude of the predicted compositional stresses (Fig. 1) we incorporate viscosity when investigating natural profiles to assess the possibility of stress relaxation via crystal plasticity.

4.2. *Theoretical example: model results*

Fig. 1 shows the temporal evolution of X_{Grs}, X_{Alm}, tangential stress, radial stress, and the relative chemical potential between Alm and Grs ($\mu_{Alm-Grs}$) for models with and without compositional stress. The other endmember mole fractions and relative chemical potentials are shown in Fig. S2.

In standard diffusion treatments without compositional stress, initial chemical heterogeneities will completely homogenize at equilibrium. In contrast, when compositional stress is included, the heterogeneities diminish but persist indefinitely, even as the garnet approaches equilibrium (Fig. 1). Without appreciating the role of compositional stress, the enduring sharp compositional contacts between mineral zones and

smaller compositional oscillations would suggest a rapid timescale (little or no diffusional relaxation) even though significant relaxation has occurred and the true timescale is much longer.

Compositional fluctuations and discontinuities can persist because the diffusion of species with different ionic radii strain the crystalline lattice, creating stresses that affect the underlying relative chemical potentials (Larché and Cahn, 1982). As relative chemical potential is a function of both composition and stress, equilibrium is achieved when the composition and stress together lead to uniform relative chemical potentials (Larché and Cahn, 1985). In both models, the $\mu_{Alm-Grs}$ profiles relax following expected diffusion behavior. Thus, despite the heterogeneity in composition and stress, the relative chemical potential approaches uniformity (and therefore no gradient) near equilibrium.

The co-existence of diffuse, wider features and heterogeneous narrow features is represented well in Fig. 1 at the 100 kyr timescale. The wider features are similar between the solutions with and without compositional stress because stresses are only beginning to develop at the longer length scales. However, compositional stresses have fully developed at shorter length scales because the relative chemical potentials have relaxed over these length scales. Consequently, in contrast to the standard model, sharp, narrower compositional features persist because of the compositional stress.

Compositional stress in garnet arises primarily due to variation in initial X_{Grs} content because the Grs endmember has a molar volume that is approximately 6–10% larger than the other endmembers (Holland and Powell, 2011). In a spherical geometry, the stress is initially dominated by the tangential stress component (Fig. 1). As diffusion proceeds, the magnitude of the radial stress component increases with time. In a planar geometry (see Profile 3 below), the change in stress is entirely due to the interface-parallel stress components, with the normal stress component remaining constant.

The profile in Fig. 1 is taken along the radial direction from garnet core to rim. The radial stress, therefore, must be continuous along the profile to satisfy force balance. The tangential stress, however, is neither required to be continuous in the radial direction nor is it (Fig. 1). If compositional zones are initially separated by a sharp composition change, tensile stress will form on one side whereas compressive stress will form on the other due to relative lattice expansion or contraction. This creates sharp changes or steps in tangential stress in the radial direction. This also means that the mean stress (an average of the tangential and radial stresses) can contain sharp discontinuities as shown in later figures.

The intracrystalline stress variations are predicted to reach or exceed ±500 MPa in garnet given initial variations of ≥0.1 X_{Grs}. Such large stresses could lead to brittle failure or plastic deformation (e.g., Cui et al., 2012; Erdélyi and Schmitz, 2012; Rogowitz et al., 2023; Scheidl et al., 2014; Yamato et al., 2019).

4.3. Natural example: sample description

To test the predicted effects of compositional stress on chemical diffusion, we examine a well-characterized garnet that exhibits extremely sharp chemical variations from Glen Clova, Scotland, the type-locality for Barrovian metamorphism (Figs. 2–3; Barrow, 1893).

The garnet is from a sillimanite zone metapelitic gneiss (JAB62A) that was metamorphosed during the Grampian orogeny (location: 56° 51.09′ N, 3° 9.40′ W; Ague et al., 2001; Ague and Baxter, 2007; Vorhies and Ague, 2011). It exhibits growth zonation that generally trends from a low X_{Grs} core to a high X_{Grs} mantle back to a low X_{Grs} rim (Fig. 2a). Sm–Nd geochronology conducted on zoned garnets from the sillimanite zone demonstrates that regional garnet growth spanned ~8 Myr; core and rim ages are c. 473 and c. 465 Ma, respectively (Baxter et al., 2002). This is consistent with textural relationships indicating *syn*-deformational garnet growth during the Grampian orogeny (McLellan, 1985).

Beyond the general X_{Grs} trend observed from core to rim, there is substantial complexity involving regions that exhibit sharp, micrometer-scale oscillations between high and low X_{Grs} (Figs. 2–3). The low X_{Grs} patches within the higher X_{Grs} garnet mantle region are associated with plagioclase feldspar inclusions, suggesting that these regions were formed as garnet overgrew and replaced plagioclase feldspar. The white arrows in Fig. 2a mark examples of regions where partially replaced relic plagioclase grains are preserved. The low X_{Grs} regions have narrow, micrometer-scale high X_{Grs} bands running through them. As these bands are confined to the low X_{Grs} zones, they cannot be late-stage fractures that have been filled in. Late-stage fracture fills would crosscut other regions, if not the entire garnet. Instead, these bands must have formed on the prograde path as the garnet mantle and rim grew.

We posit that the compositional oscillations were created by fluid-mediated plagioclase replacement reactions attending prograde

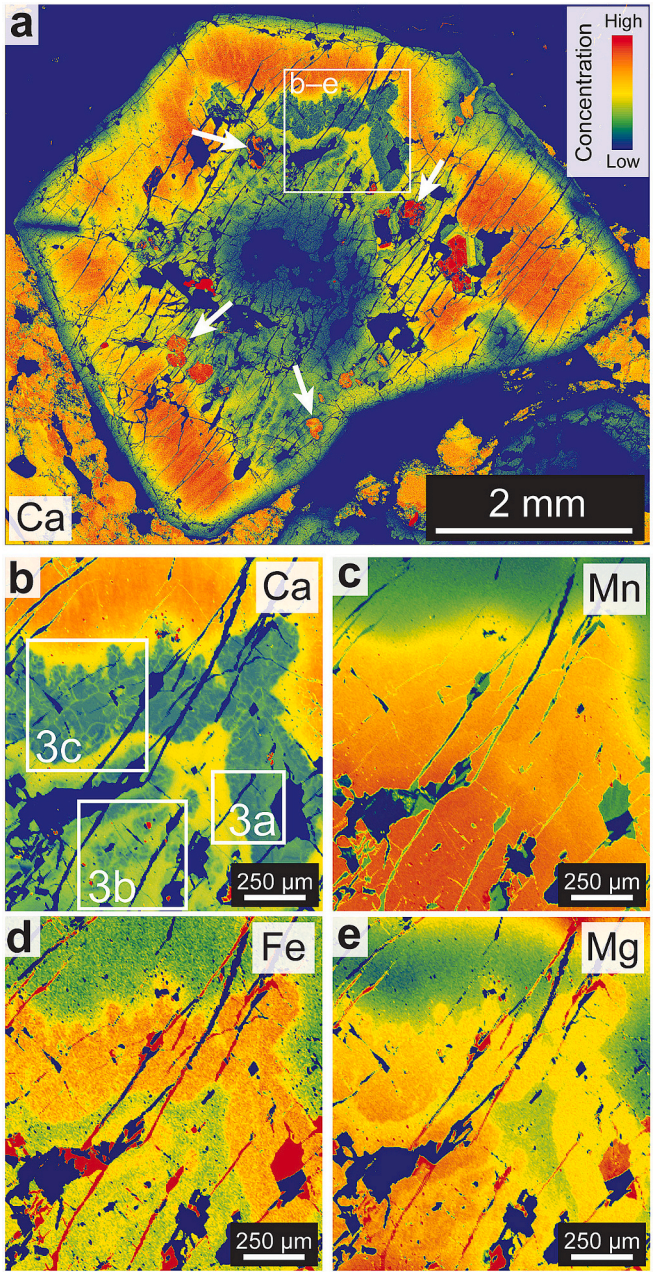

Fig. 2. Chemical maps of garnet in sample JAB62A. a) Ca map of the garnet crystal of interest modified from Vorhies and Ague (2011). White arrows show examples where partially replaced plagioclase inclusions are preserved. b–e) Higher resolution maps of Ca, Mn, Fe, and Mg of the region marked in part a. Ca preserves the most detail, whereas Mn is the most smoothed.

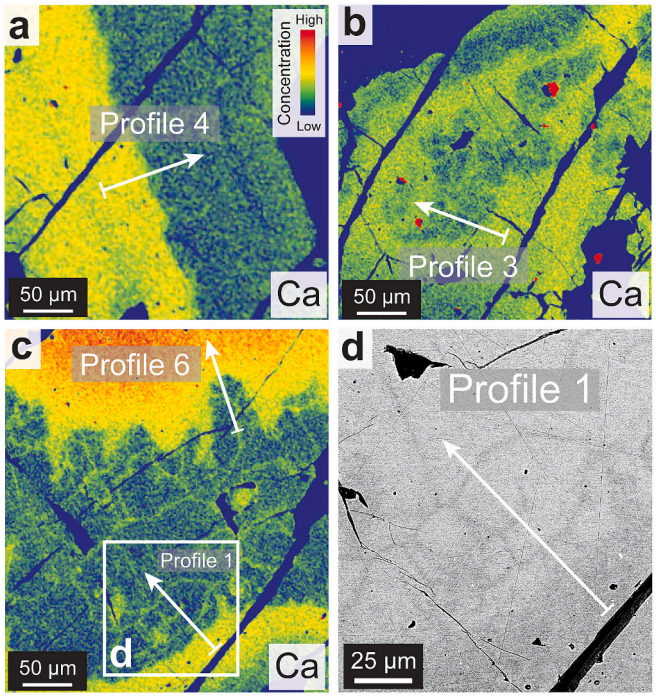

Fig. 3. Ca maps and backscatter electron (BSE) image of garnet regions marked in Fig. 2. a–c) Ca maps showing the locations of chemical profiles 1, 3, 4, and 6. Note the micrometer-scale chemical variations shown in b and c. d) A BSE image showing textures indicative of relic grain boundaries. The low Ca regions are interpreted to be caused by local replacement of plagioclase feldspar (Fig. 2a).

metamorphism and dehydration. Consistent with this interpretation, backscatter electron (BSE) imaging reveals textures indicative of relic grain boundaries between former matrix phases in the regions of significant local X_{Grs} variation (Fig. 3d). Variation in garnet chemistry as a function of the precursor phase chemistry (i.e., overprint zonation) has been previously documented in garnet (e.g., Ague and Carlson, 2013). Fluid-mediated replacement reactions are known to create extremely sharp chemical boundaries, consistent with the observed micrometer-scale compositional changes (Ague and Axler, 2016; Putnis and Austrheim, 2010).

Local equilibrium between the host garnet and plagioclase inclusions and pseudosection analysis demonstrate that the textures developed during the Grampian orogeny on the prograde path prior to peak temperature metamorphic conditions (Fig. S4; Vorhies and Ague, 2011). The interior region of the garnet mantle grew at ~550 °C and 0.4–0.5 GPa. Burial along a steep dP/dT path resulted in growth of the higher X_{Grs} mantle exterior at maximum pressures of 0.8–1.0 GPa. After considerable exhumation, the garnet rim grew at the peak temperature conditions of ~660 °C and ~0.6 GPa during thermal pulse activity (Ague and Baxter, 2007; Vorhies and Ague, 2011). Partial melt textures in some lithologies in the region suggest that temperatures reached 670–680 °C, at least locally (McLellan, 1985). Although the pseudosection does not capture the details of the plagioclase replacement reactions, it clearly shows the broad prograde pattern of low-X_{Grs} core, high-X_{Grs} mantle, and low-X_{Grs} rim (Fig. S4b). Our textural and growth history interpretations do not include garnet replacement reactions as we find no evidence for them. However, if any such reactions took place on the prograde path up to and including partial melting if it occurred, the resultant compositional variations would still have been present at peak conditions so the timescale estimate and discussion presented below would remain valid.

The approximate duration of peak temperature metamorphism has been independently constrained to be between 10^5 and 10^6 yr by multiple lines of evidence. First, strontium-in-apatite tracer diffusion systematics over a range of metamorphic zones indicate that peak temperature conditions lasted for c. 150–400 kyr (Ague and Baxter, 2007). Apatite crystals from lower grade rocks (e.g., biotite zone, 450 °C) exhibit distinct, sharp Sr zonation. As metamorphic grade increases, the Sr zonation is progressively smoothed from the garnet zone (535 °C) to the staurolite zone (595 °C) to the sillimanite zone (660 °C) (Fig. S5). Crucially, Sr profiles in apatite crystals from the sillimanite zone are homogenized, thus independently constraining the *minimum* timescale of peak metamorphism in this study to be >100 kyr (Fig. S5; Ague and Baxter, 2007).

Given that many apatite crystals were analyzed, any variation in diffusion rates due to crystallographic orientation effects (which, if present, are small; Cherniak and Ryerson, 1993) is encapsulated in the spread of the 150–400 kyr estimated range. In addition, the presence or absence of water has little effect on Sr diffusion rates in apatite (Watson and Baxter, 2007). Importantly, the consistency of peak temperature timescale estimates and the progressive smoothing of apatite Sr profiles with grade indicate that peak temperature metamorphism occurred penecontemporaneously across the metamorphic zones, consistent with Sm–Nd garnet geochronology (Ague and Baxter, 2007; Baxter et al., 2002).

Likewise, garnet diffusion chronometry estimates from other nearby sillimanite grade rocks (samples JAB60A and JAB61A) similarly constrain the timescale to >100 kyr. Ague and Baxter (2007) obtain a peak temperature timescale of 110 kyr from garnet based on the relaxation of internal chemical zonation (sample JAB60A). Consistently, we estimate a timescale of 200 kyr based on the length scale of garnet rim diffusion (Fig. S6; sample JAB61A). The approximately 200 kyr time is a minimum as any dissolution occurring during diffusion would lead to an underestimation of the true timescale (e.g., Kohn and Spear, 2000).

The c. 100–400 kyr duration of peak temperature conditions was due to a thermal pulse or pulses from late-stage magma advection superimposed on the background Grampian orogenic event (Ague and Baxter, 2007; Baxter et al., 2002; Viete and Lister, 2017; Vorhies and Ague, 2011). Thermal conduction modeling likewise indicates that regional heating at the scale of the Barrovian metamorphic zones requires ≥100 kyr at or near peak temperature conditions (Fig. S7; Viete and Lister, 2017). Thus, thermal modeling and multiple diffusion chronometers all constrain the timescale to approximately 100–400 kyr for peak temperature metamorphism for this sample (Figs. S5–S7).

4.4. Natural example: modeling results

The well-characterized pressure-temperature-time history combined with the extremely sharp, micrometer-scale changes in garnet X_{Grs} make this an excellent candidate for applying compositional stress theory. We present four chemical profiles measured via EPMA with 1 μm spacing (Figs. 4–7). The profiles record large X_{Grs} changes over single micron steps. The fluctuations are almost certainly sharper than measured (i.e., sub-micron) owing to EPMA beam convolution effects (Fig. S1). The sharpness of these features could be further constrained by collecting more tightly spaced EPMA profiles and applying deconvolution methods or by examining contrast changes in higher resolution BSE images (e.g., Ganguly et al., 1988; Spear et al., 2012; Chu et al., 2017).

We fit the observed profiles at peak temperature conditions of 660 °C and 0.6 GPa using (1) a standard diffusion treatment that does not include compositional stress (e.g., Ague and Baxter, 2007; Borinski et al., 2012; Faryad and Chakraborty, 2005) and (2) our treatment that incorporates compositional stress theory. The geometry of each profile is approximated as either spherical or planar, depending on the orientation of the transect. This is justified because deviations from a spherical or planar approximation will not in general change the stress type predicted: decreases in X_{Grs} will create tensile stress and increases in X_{Grs}, compressive stress (Larché and Cahn, 1982). Consequently, although accounting for the more complex shapes of the regions may change the

modeled stress magnitudes and the best-fitting initial conditions somewhat, the fundamental effects of this stress on chemical diffusion remain unchanged and our results would not be appreciably altered. We also employ zero flux boundary conditions because the features being modeled are in the garnet mantle and formed prior to peak temperature conditions. Therefore, we assume that there was no communication between the regions of interest and the matrix during diffusion.

The initial conditions for each profile represent fit parameters that were solved for by using Monte Carlo forward modeling. We assume that the composition in each profile oscillates between high and low X_{Grs} values bounded between approximately $X_{Grs} = 0.06$ and 0.21. This range encapsulates the highest and lowest X_{Grs} values observed within the garnet and is consistent with general thermodynamic expectations for the given pressure and temperature range experienced by this sample (Fig. S4). Moreover, the profiles show that there is substantial compositional variation at the micrometer scale within both the high and low X_{Grs} regions. This is likely due to kinetic limitations on element availability during garnet formation and variations in local chemistry in the phases being replaced (e.g., Ague and Carlson, 2013). The goodness of fit for each profile was determined by calculating the standard deviation of the X_{Grs} and X_{Alm} residuals (SDRs) between the observed data and our modeled profile. Only the X_{Grs} and X_{Alm} residuals are used because Grs and Alm record the dominant compositional variation.

The timescale of peak temperature metamorphism was determined from Profile 4 which records interdiffusion between two distinct compositional zones (Fig. 4). Profile 4 demonstrates that the best-fitting timescale is similar regardless of compositional stress: model results give a duration of 180 kyr with compositional stress and 125 kyr without (Fig. 4). The SDR for the Profile 4 best fit with stress was 0.0038 (2σ) and without stress was 0.0046 (2σ). Although the best fit with compositional stress is better than without, these values are not significantly different ($p = 0.26$) using an F-test for equality of variances.

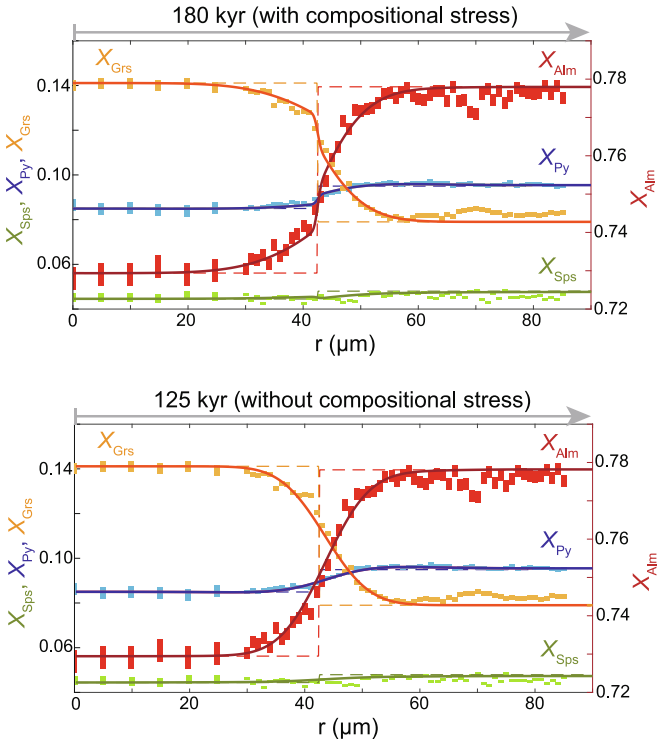

Fig. 4. Best-fitting modeled diffusion profiles for Profile 4. Diffusion is modeled with compositional stress (top) and without compositional stress (bottom). Linear viscous relaxation is incorporated into the model with compositional stress. The dashed lines are the initial conditions (IC), the solid lines are the final model results, and the rectangles are the measured data points (heights are $\pm 2\sigma$ uncertainty). The timescales obtained from the best-fitting models for peak metamorphic conditions are 180 kyr (top) and 125 kyr (bottom).

We use the 180 kyr time when fitting the remaining profiles, but the following results and discussion would not change significantly if the 125 kyr time were used instead. Both results are also consistent with the timescale determined by independent diffusion and thermal conduction modeling (Figs. S5–S7). The SDRs for the compositional stress model were iterated to 0.0034, 0.0030, and 0.0044 (2σ) for Profiles 1, 3, and 6, respectively. In contrast, the SDRs for the standard diffusion treatment are 0.0066, 0.0052, and 0.0078 (2σ) for Profiles 1, 3, and 6, respectively. The SDRs for the compositional stress fits are smaller than those for the corresponding standard fits at the statistical significance level of $p < 1 \times 10^{-7}$ using an F-test for equality of variances. Thus, the compositional stress fits are clearly superior both visually and statistically (Figs. 4–7).

5. Discussion

5.1. Compositional stress and diffusional relaxation

The discussion below deals primarily with the grossular component as it illustrates the effects of compositional stress particularly well, having the largest molar volume, the largest compositional range, and the highest analytical measurement precision in this study.

Additionally, it is important to emphasize that our focus is on the total extent of diffusional relaxation. A timescale of 180 kyr for peak temperature conditions captures the total amount of diffusional relaxation observed. If we use instead a "characteristic temperature" of 640 °C which approximates diffusion over a time-integrated cooling path (e.g., Chakraborty and Ganguly, 1991), then the diffusional relaxation is estimated to have occurred over approximately 450 kyr. However, the total extent of diffusional relaxation is identical in either case and therefore makes no difference for our goal of examining the effects of compositional stress on diffusion profiles.

Modeling diffusion with compositional stress provides far better fits to the observed data than a standard diffusion model for Profiles 1, 3, and 6. The significantly poorer quality of fit using the standard treatment results primarily from its inability to reproduce the smaller wavelength compositional features in the data at the 180 kyr timescale of peak temperature metamorphism (Figs. 5–7).

The difference between these models stems from the underlying relative chemical potential gradients which provide the driving force for diffusion (Hess and Ague, 2023; Larché and Cahn, 1982, 1985). In both models, the relative chemical potential profiles relax following classical diffusion behavior and are approximately the same (Figs. 1, 8). However, in standard diffusion models, pressure is assumed to remain constant, meaning that the relative chemical potentials are only a function of the composition. In contrast, when compositional stress is included, the relative chemical potentials are a function of both composition and stress. Consequently, the composition profiles evolve differently even as the relative chemical potential profiles are nearly identical (Fig. 1).

Fig. 9a demonstrates the exponential relationship between the characteristic length scale of diffusional relaxation and inferred diffusion timescales. We define the characteristic length scale $L = 4\sqrt{Dt}$ where D is an interdiffusion coefficient (Fig. 9a; Philpotts and Ague, 2022). In standard diffusion models, a characteristic diffusion length scale of, for example, 20 μm in the relative chemical potential profile will correspond to a relaxation length scale of 20 μm in the composition profile. It necessarily follows that shorter, micrometer-scale compositional oscillations will be completely relaxed by the time the 20 μm characteristic length scale has been reached (Figs. 1, 9).

Thus, it is not possible in standard diffusion models for the 1–2 μm compositional variations observed in the measured profiles to persist given the ~20 μm characteristic length scale of diffusion indicated, for example, by Profile 4 (Figs. 4, 9b). This problem is independent of diffusion coefficient calibration. Although we use the calibration of Chu

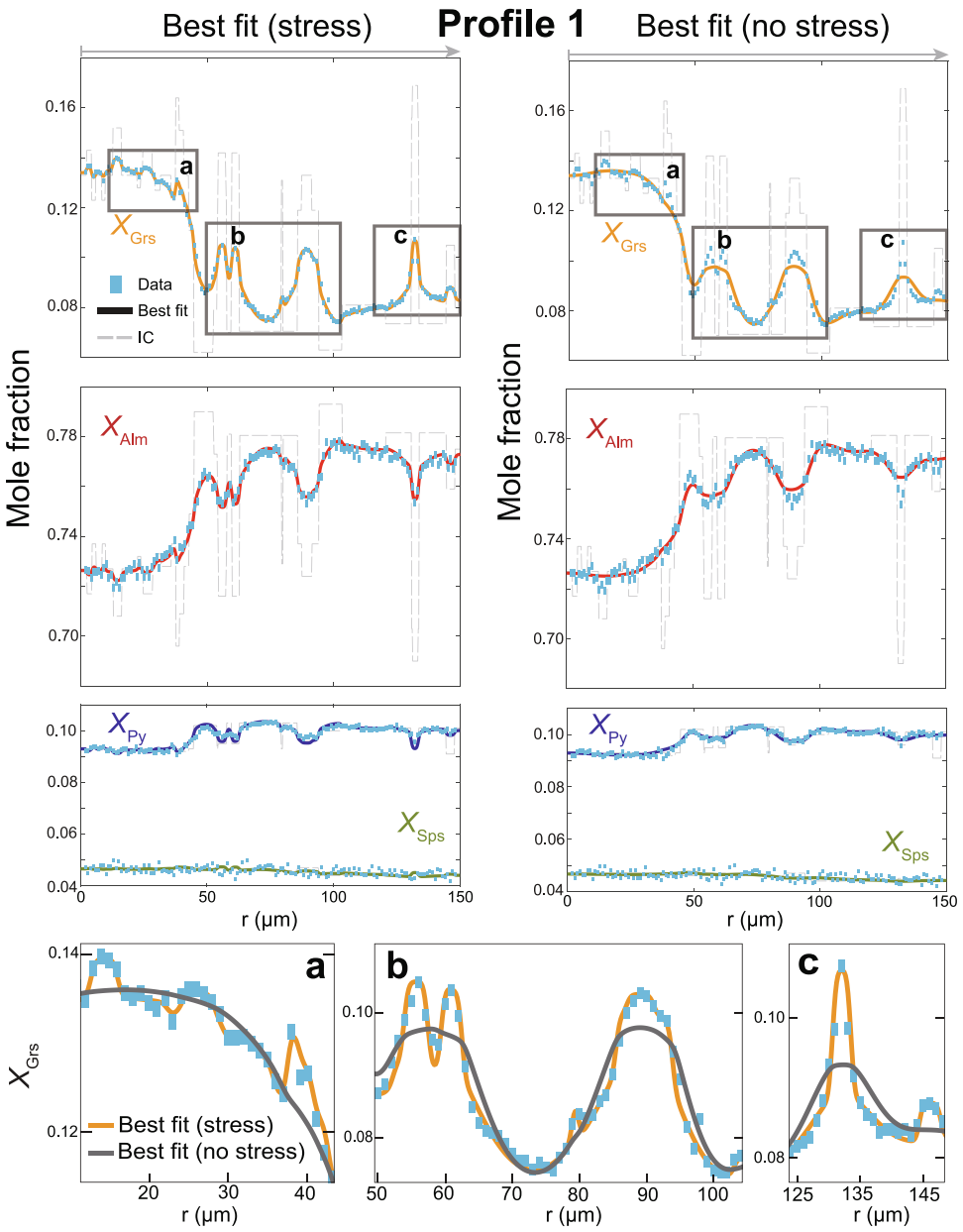

Fig. 5. Data and model results for Profile 1. Diffusion is modeled at peak temperature conditions for 180 kyr using a spherical geometry. The left panels show the best-fitting model results with compositional stress, and the right panels, without. The thin dashed lines are the initial conditions (IC), the thick lines are the best-fitting model results, and the blue rectangles are the measured data (heights are $\pm 2\sigma$ uncertainty). The panels marked a, b, and c show zoomed in regions comparing the best-fitting model results for the Grs endmember. (For interpretation of the references to colour in this figure legend, the reader is referred to the web version of this article.)

and Ague (2015) and Chen and Chu (2024), the same inconsistency in observed diffusion length scales would arise using any other diffusion coefficient calibration.

When compositional stress is included, however, the relaxation of the compositional heterogeneities gives rise to compositional stresses which also affect relative chemical potential. Consequently, if the relative chemical potentials are relaxed at a characteristic length scale of 20 μm but there are variations in stress at the micrometer scale, then the compositional profile must also be heterogeneous at the micrometer scale (Figs. 1, 8).

The relationship between length scale, stress, and composition can then explain the observed features in the measured composition profiles (Figs. 4–7). The diffusion length scale is inferred to be approximately 20 μm (Figs. 4, 9b). The larger compositional variations at this length scale are beginning to relax but have not fully relaxed. As a result, substantial compositional stresses have not fully developed at this length scale (Fig. 8), and therefore, the diffusion model results with and without compositional stress appear similar in shape. Hence, the broad shapes of the features in Profiles 1, 3, and 6 are similar with or without compositional stress (Figs. 5–7).

But the longer characteristic length scale means that the relative chemical potential variations must be relaxed at the micrometer-scale (Figs. 8 and 9). However, this relaxation gives rise to significant compositional stresses. The only way to have relaxed relative chemical potentials at the micrometer scale when there are stress variations is for the composition to also be heterogeneous. Consequently, although there are features that have diffuse appearances at the 20 μm length scale, there are also (necessarily) sharp compositional heterogeneities at the micrometer-scale (Fig. 8). This apparent dichotomy is the hallmark of diffusional relaxation in crystals affected by compositional stress.

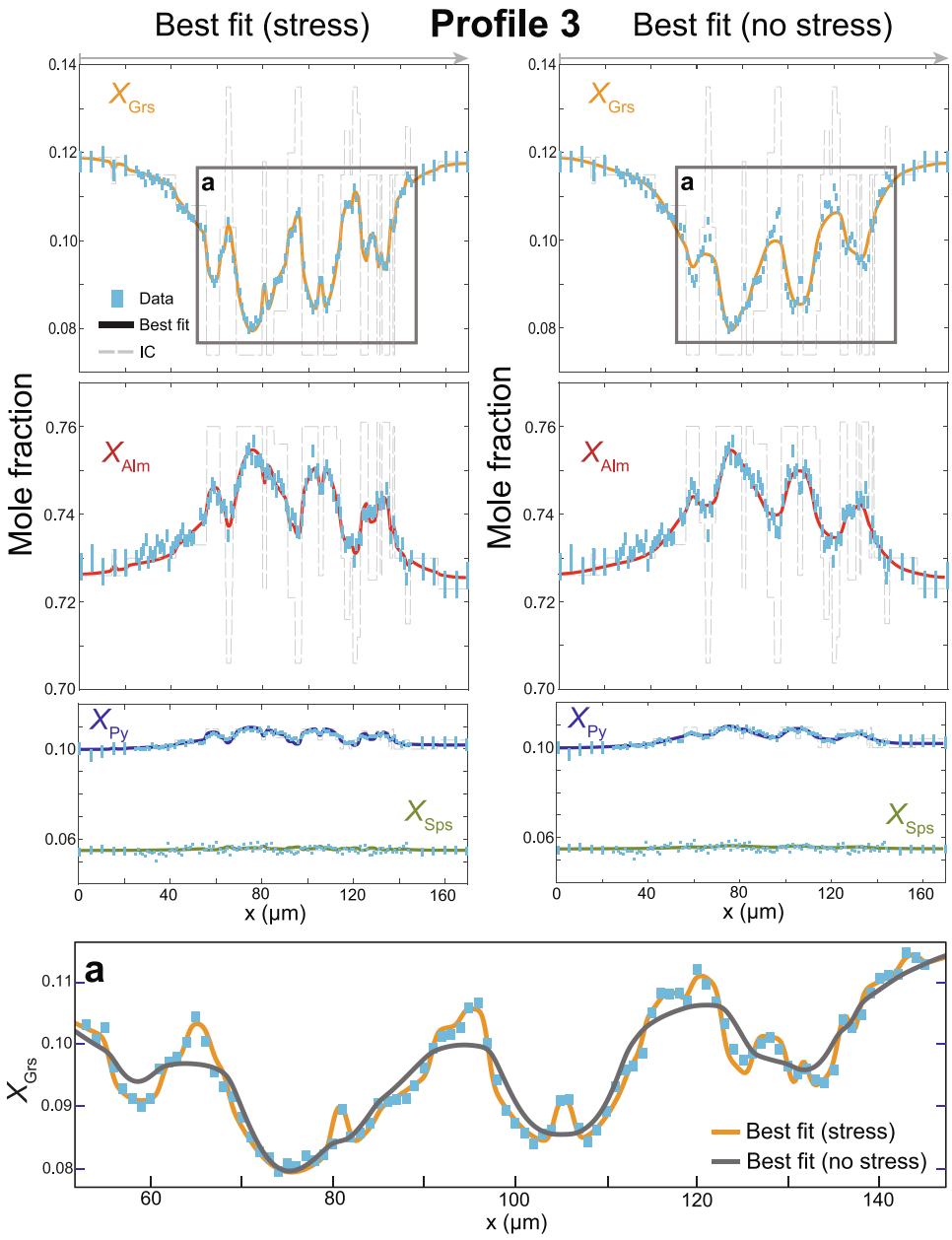

Fig. 6. Data and model results for Profile 3. Diffusion is modeled at peak temperature conditions for 180 kyr assuming a planar geometry. The left panels show the best-fitting model results with compositional stress, and the right panels, without. The thin dashed lines are the initial conditions (IC), the thick lines are the best-fitting model results, and the blue rectangles are the measured data (heights are $\pm 2\sigma$ uncertainty). The panel marked a shows a zoomed in region comparing the best-fitting model results for the Grs endmember. (For interpretation of the references to colour in this figure legend, the reader is referred to the web version of this article.)

Compositional stress suggests that one could incorrectly infer a maximum peak thermal timescale given by the characteristic relaxation timescale of the smallest compositional heterogeneities or sharpest compositional contacts. The micrometer-scale compositional oscillations observed in our data, for example, require a maximum timescale of about 1–10 kyr using a standard diffusion treatment (Fig. 9b). However, this contradicts both the longer diffusion timescales indicated by the measured chemical profiles and the independent constraints on the minimum timescale given by homogenized Sr profiles in apatite and garnet rim diffusion length scales observed in other sillimanite zone samples (>100 kyr; Figs. S5–S6). Furthermore, it is geodynamically unfeasible for the entire sillimanite zone (>10 km length scale; Barrow, 1893) to be heated and cooled in $\sim 10^3$ yr even for the Barrovian case of a rapid thermal pulse or pulses associated with conductive heating from magma advection followed by thermal relaxation (Ague and Baxter, 2007; Viete and Lister, 2017; Vorhies and Ague, 2011). Thermal modeling shows that the region must have been at peak temperature for >100 kyr (Fig. S7; Viete and Lister, 2017). Thus, the 1–10 kyr timescale suggested by the sharpest compositional oscillations is unlikely.

In summary, compositional stress theory provides an explanation for the observed micrometer-scale compositional variations and unifies them under a longer timescale that is consistent with independent constraints on the minimum duration of peak temperature metamorphism (Figs. 4–7 and S5–S7). Therefore, compositional stress could change the interpreted timescale of diffusional relaxation by potentially orders of magnitude (Figs. 9–10).

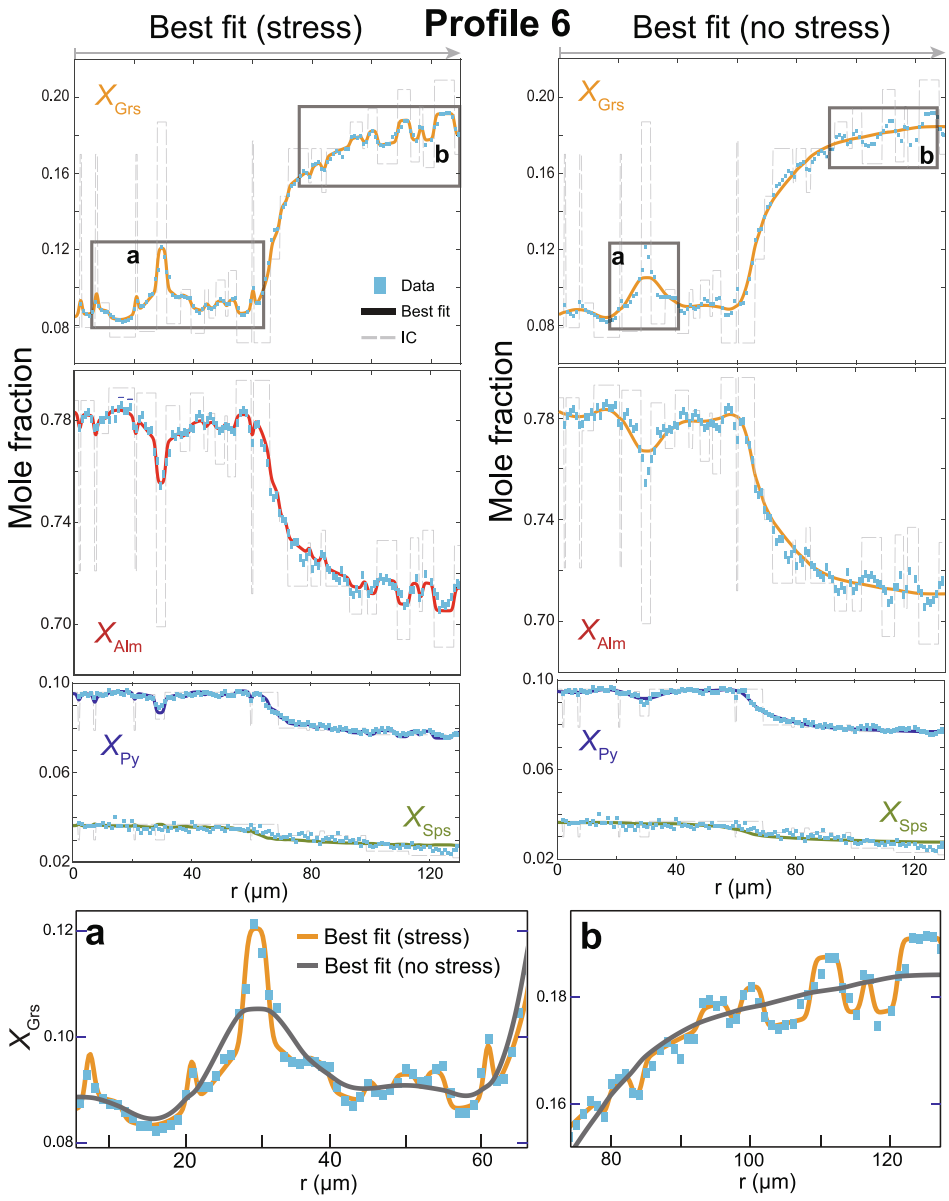

Fig. 7. Data and model results for Profile 6. Diffusion is modeled at peak temperature conditions for 180 kyr assuming a spherical geometry. The left panels show the best-fitting model results with compositional stress, and the right panels, without. The thin dashed lines are the initial conditions (IC), the thick lines are the best-fitting model results, and the blue rectangles are the measured data (heights are $\pm 2\sigma$ uncertainty). The panels marked a and b show zoomed in regions comparing the best-fitting model results for the Grs endmember. (For interpretation of the references to colour in this figure legend, the reader is referred to the web version of this article.)

5.2. *Diffusion rates, deformation, and alternate formulations*

Compositional stress may have additional impacts on solid solution minerals beyond changing diffusion profile morphology. Larché and Cahn show that compositional stress results in faster diffusion (Larché and Cahn, 1982). Although the diffusion coefficients remain constant, the stress somewhat increases the magnitude of the relative chemical potential gradients that drive diffusion, and hence, the apparent rate of diffusion increases. Our treatment incorporates this effect; diffusion rates for garnet increase by a few percent when compositional stress is included compared to standard diffusion models. This was determined by comparing the diffusion length scales (Fig. S8). This change is small, particularly in comparison to the uncertainties on the diffusion coefficients themselves (approximately ± 0.3 $\log_{10}$ units, 1σ; Chu et al., 2017). Nonetheless, stress-enhanced diffusion rates might be larger and more important in other network solids (e.g., Tomozawa and Davis, 1999).

Compositional stress may drive other fundamental processes such as irreversible plastic deformation (Erdélyi and Schmitz, 2012; Stephenson, 1988; Zhong et al., 2017). Consequently, we have included linear viscous relaxation in our stress models. While plastic deformation (i.e., dislocation creep) in garnet exhibits a power-law behavior ($n \approx 3$) as a function of deviatoric stress (Karato et al., 1995; Wang and Ji, 1999), the assumption of linearity provides an initial basis to consider the possibility of viscous relaxation.

Garnet flow properties have been experimentally determined at high temperatures and strain rates and suggest a viscosity of approximately 10^{22}–10^{23} Pa·s at the pressure, temperature, and differential stress conditions of this study (Karato et al., 1995; Wang and Ji, 1999). However, Wang and Ji (1999) also indicate that steady-state flow laws

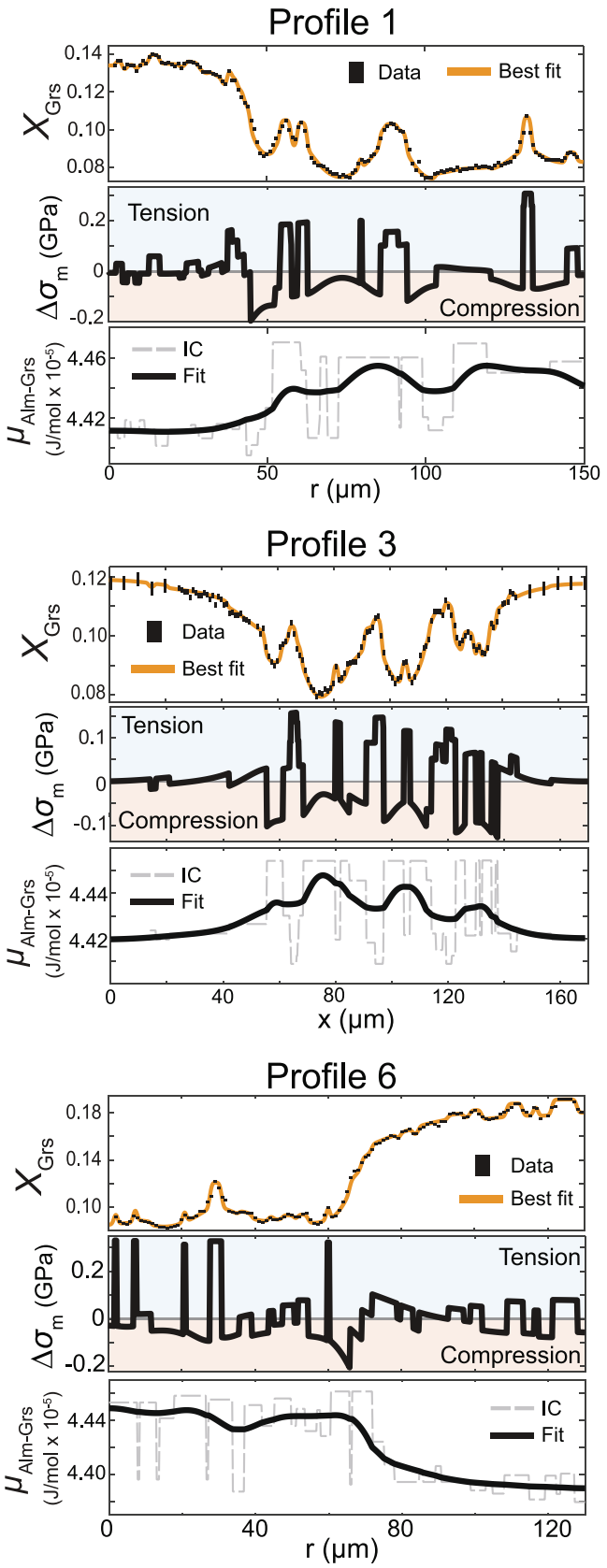

Fig. 8. Plots of X_{Grs}, final change in mean stress ($\Delta\sigma_m$), and relative chemical potential between Alm and Grs ($\mu_{Alm-Grs}$) for Profiles 1, 3, and 6. Relative chemical potential drives diffusion and is a function of both composition and stress. Note that the relative chemical potential plots are smooth even though sharp, micrometer-scale oscillations exist in composition and stress.

cease to hold for temperatures <750–800 °C, at which point the strength of garnet apparently increases by several orders of magnitude.

We find that a viscosity lower than 10^{24} Pa·s causes the smallest observed micrometer-scale compositional features to relax at a 100 kyr timescale. Thus, garnet likely has a viscosity $\geq 10^{24}$ Pa·s at these pressure-temperature conditions, consistent with the analysis of Wang and Ji (1999). The strength of garnet may even be significantly higher as natural and experimental studies suggest that garnet can sustain hundreds of MPa up to GPa-level differential stresses over geological timescales as indicated by preservation of coesite inclusions in garnet, deformation experiments, and elastic inclusion barometry studies (e.g., Parkinson, 2000; Rogowitz et al., 2023; Yamato et al., 2019; Zhong et al., 2019).

Crystal plasticity and annealing may, however, explain why the effects of compositional stress have not previously been reported in garnet diffusion-couple experiments (e.g., Borinski et al., 2012; Ganguly, 2010). These experiments are typically conducted at high temperatures (i.e., ≥1000 °C) where rates of irreversible deformation and crystal annealing may exceed that of diffusional relaxation (Wang and Ji, 1999). In addition, as temperature increases, solid solutions become more ideal and mixing is increasingly favored (White et al., 2014). Consequently, the mixing term in relative chemical potential becomes larger relative to the stress term, and so larger stresses are required to alter the mineral composition. As such, the effects of compositional stress on diffusional relaxation will become more subtle (Hess and Ague, 2023; Hess et al., 2022). Thus, the influence of compositional stress may be much less apparent in high-temperature diffusion experiments than in natural garnets formed at appreciably lower temperatures.

Finally, Zhong et al. (2017) provide an alternative formulation for coupling chemical diffusion and compositional stresses in binary mineral solid solutions based on irreversible fluid thermodynamics (Tajčmanová et al., 2021). It does not incorporate the network constraint imposed by crystalline lattices and, thus, is at variance with Larché-Cahn theory (Hess et al., 2022; Tajčmanová et al., 2021). We are unable to evaluate this approach further at present, as considerable theoretical development is necessary to apply it to multicomponent diffusion in ionic crystals (e.g., garnet), which is beyond our scope here.

5.3. *Implications*

We have developed and applied compositional stress theory to garnet and have examined the essential theoretical predictions using a well-characterized natural sample as a case study. As the theory is general in its treatment of the interactions of stress and chemical diffusion, its implications are relevant to diverse metamorphic and igneous systems.

First and foremost, the results predict that compositional stress can prevent chemical features from fully relaxing in the absence of crystal plasticity (Fig. 1). Consequently, chemical profiles that suggest rapid timescales based on sharp zonal contacts or persistent short-wavelength compositional features could represent much longer timescales when compositional stress is accounted for (Fig. 9).

A quantitative test of this hypothesis is provided by chemical zoning preserved in garnet from Glen Clova, Scotland. Independent diffusion and thermal modeling for this locality indicate that peak temperature metamorphism lasted 100–400 kyr (Figs. 4, 9, and S5–7). Nonetheless, the high-resolution garnet chemical profiles contain sharp chemical oscillations that imply a maximum peak temperature timescale of about 1–10 kyr using a standard diffusion treatment (Figs. 5–9). Compositional stress offers an explanation for the persistence of these features for 180 kyr, consistent with both the longer characteristic length scales present in the profiles and with independent timescale constraints. Thus, compositional stress could change diffusion chronometry-based timescale estimates by orders of magnitude, offering a viable interpretation for some instances of discrepancies between diffusion chronometry and isotope geochronology (Fig. 10; Viete and Lister, 2017).

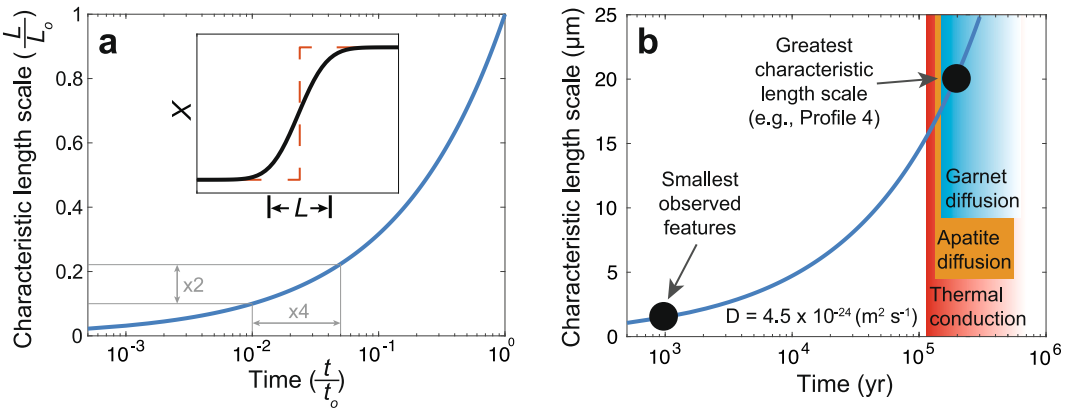

Fig. 9. Characteristic length scale for significant diffusion (L) as a function of time (t). a) Non-dimensional characteristic length scale (L/L_0) plotted against non-dimensional time (t/t_0). The L value is defined as $L = 4\sqrt{Dt}$ where D is an interdiffusion coefficient (Philpotts and Ague, 2022). L approximates the width of an initially sharp contact undergoing diffusional relaxation (inset). b) Plot of characteristic time versus length scale using the diffusion coefficient calibration of Chu and Ague (2015). As diffusion primarily occurs between Alm and Grs, we use an Alm–Grs interdiffusion coefficient ($D_{Alm–Grs}$ of 4.5×10^{-24} m^2 s^{-1}) for a representative garnet composition of $X_{Alm} = 0.75$, $X_{Py} = 0.1$, $X_{Grs} = 0.1$, $X_{Sps} = 0.05$ and the peak temperature, pressure, and oxygen fugacity of this study (main text). In a standard diffusion treatment, the smallest micrometer-scale compositional features should relax long before reaching the timescale suggested by the features with the greatest characteristic length scale (180 kyr) and by other independent time constraints.

Although this study focuses on the preservation of sharp, oscillating features, compositional stress similarly impacts chemical profiles with single, sharp composition changes between zones. Sharp composition changes across mineral zones will persist indefinitely in the absence of significant intracrystalline deformation (Fig. 1). Thus, a sharp zone contact could be consistent with a much longer metamorphic timescale. Nonetheless, a timescale can still be inferred from the width of the diffusion limbs on either side of the contact (Fig. 9).

The effects of compositional stress on major element diffusion will be most relevant when interdiffusion occurs between species with substantially different endmember molar volumes or lattice parameters (i.e., several percent or greater difference). This offers a first order estimate as to whether compositional stress is likely to be important. For example, grossular is 6–10% larger than almandine, pyrope, or spessartine, and as a result the compositional stress effects are large (Fig. 1; Holland and Powell, 2011). Similar effects might arise for substitutions involving other garnet endmembers with large molar volumes such as andradite.

Compositional stress is thus likely to be important in garnets from high-grade metamorphic rocks in subduction zone (i.e., blueschist and eclogite facies) and Barrovian metamorphic settings (i.e., amphibolite facies), as they often have relatively large variations in X_{Grs} and are hot enough for significant intracrystalline diffusion (i.e., ≥600 °C, depending on the timescale). However, at granulite or ultrahigh-temperature metamorphic conditions (>800 °C), the extent to which the predicted stress effects will be diminished or absent due to viscous relaxation is unknown. Careful examination of garnets which experienced these conditions may offer important insights into the role of viscous relaxation at such temperatures. We note in this context that observing the influence of compositional stress in any metamorphic setting will generally require chemical profiles and maps with a high spatial resolution and a mindfulness of convolution effects because the stress acts to preserve extremely sharp chemical contacts (Fig. 1 and S1–S2).

In contrast, compositional stress effects will typically be minor when the diffusing major elements have similar endmember molar volumes. For example, the molar volume difference between Alm and Py is one tenth of the difference between Grs and Py (Holland and Powell, 2011). Consequently, a much larger initial difference in Alm and Py (e.g., ≥0.2 mole fraction) is required to generate appreciable intracrystalline stresses (e.g., ≥100 MPa) via diffusion. Thus, for most cases of primarily Mg–Fe interdiffusion in garnet, classical treatments will provide reliable results (e.g., Borinski et al., 2012; Devoir et al., 2021; Ganguly, 2010; Spear, 1991).

Our focus has been on major element diffusion, but what effects might stress have on trace elements? Trace element partition coefficients and diffusion rates have been shown to be a function of the element's size (Blundy and Wood, 2003; Cherniak and Watson, 2003; Van Orman et al., 2001). Thus, trace element diffusion could plausibly be affected by compositional stress. Although trace element diffusion itself is unlikely to generate significant stress, compositional stresses generated by major elements might nonetheless affect trace element diffusion. Just as large compositional stresses will prevent major element zonation from fully relaxing (Fig. 1), we suggest that trace elements could also record enduring chemical zonation due to these compositional stresses. Extending compositional stress theory to trace element-bearing species, however, would require knowledge of their standard-state thermodynamic properties, activity-composition relationships, substitution mechanisms, diffusion rates, and volumetric and mechanical properties. Although beyond our scope here, this represents an important area for future experimental and theoretical investigation, as trace element diffusion behaviors are important for diffusion chronometry, geochronology, and geochemical modeling of petrologic processes (e.g., Ague and Baxter, 2007; Bloch et al., 2020; Blundy and Wood, 2003; Cheng et al., 2008; Costa et al., 2003; Cruz-Uribe et al., 2015; Ruprecht and Plank, 2013; Smye et al., 2017; Watson and Baxter, 2007).

Beyond timescales and chemistry, compositional stress may also affect techniques such as inclusion barometry. The stress states of mineral inclusions relative to their hosts can be used to infer pressure and temperature conditions of entrapment (e.g., Kohn, 2014; Murri et al., 2018). However, compositional stress can change internal stresses by several hundred MPa (Figs. 1, 8) which would alter inclusion barometry results if not accounted for. The potential for viscous relaxation of the host mineral is an additional concern (e.g., Dabrowski et al., 2015). In this study we find the observed compositional features can only be explained if garnet has a viscosity of $\geq 10^{24}$ Pa·s at the investigated pressure and temperature conditions. Thus, the persistence of short-wavelength compositional features relative to the inferred timescale of diffusion can offer independent natural constraints on mineral strength.

Accounting for compositional stress in solid solutions may alter our interpretations of igneous and metamorphic events. Here, we have examined the essential aspects of compositional stress theory and shown that it can alter interpreted timescales by an order of magnitude or more. We have also discussed additional implications for other standard petrological techniques. Further investigation of compositional stress in multicomponent minerals has great potential to provide new,

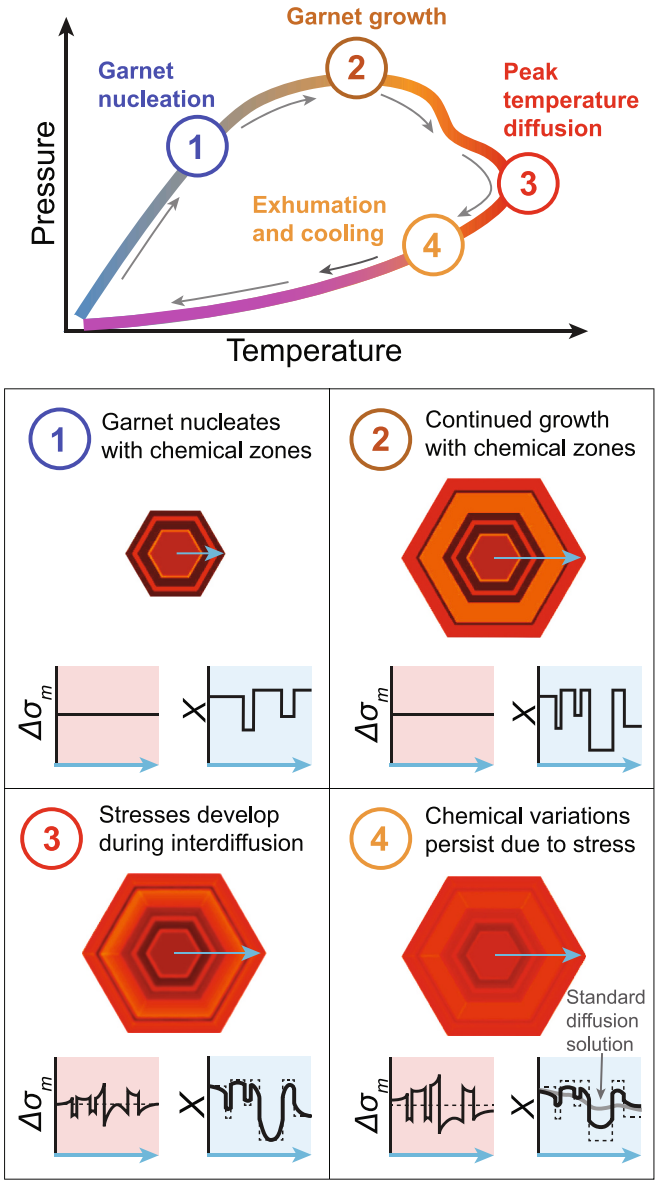

Fig. 10. Expected garnet growth and diffusion behavior with compositional stress. Garnet in a rock following a pressure-temperature pathway nucleates (1), grows (2), undergoes intracrystalline diffusional relaxation during peak temperature metamorphism (3), and is exhumed (4). Differences in endmember mole fraction (X) between initial sharp mineral zones result in diffusional relaxation which is used to infer the timescale of high temperature metamorphism. However, if diffusion occurs between cations with different sizes, intracrystalline stresses will develop ($\Delta\sigma_m$). The stress will prevent the initial composition boundary from fully relaxing as shown in (3) and (4) in the absence of intracrystalline plastic deformation. The dashed lines in (3) and (4) indicate initial conditions and the gray line in (4) indicates the expected composition profile when compositional stress is not included (inset graphs). Although the composition differences at zone contacts diminish, they are not eliminated because of compositional stress even when the garnet is near equilibrium. Thus, without consideration of compositional stress, one would incorrectly conclude that the timescale was much shorter than it actually was.

multifaceted insights into the timescales and physical conditions of lithospheric processes.

CRediT authorship contribution statement

Benjamin L. Hess: Writing – review & editing, Writing – original draft, Visualization, Validation, Supervision, Software, Resources, Project administration, Methodology, Investigation, Funding acquisition, Formal analysis, Data curation, Conceptualization. **Jay J. Ague:** Writing – review & editing, Writing – original draft, Visualization, Validation, Supervision, Software, Resources, Project administration, Methodology, Investigation, Funding acquisition, Formal analysis, Data curation, Conceptualization.

Declaration of competing interest

The authors declare no competing interests.

Data availability

The data that support the findings of this work are available within the article and its supplementary material files. The codes used to produce the results and figures presented in this work are also available in the supplementary files provided with this paper. The MATLAB® software package was used for calculations and data analysis. The Probe Software package (https://probesoftware.com) was used for quantitative EPMA data acquisition and analysis.

Acknowledgments

We thank M.T. Brandon, A.A. Haws, J. Neuhoff, P.W. Voorhees, S. Piazolo, and C. Xu for thoughtful discussions; H. Cheng and F. Spear for their thorough and constructive reviews; J. Wheeler and E. Bloch for their critical and constructive comments on an earlier version of the manuscript; and J.O. Eckert, Jr., for valuable assistance with the EPMA. Financial support from the US National Science Foundation Directorate of Geosciences (EAR-2208229) and Yale University are gratefully acknowledged.

Appendix A. Supplementary data

Supplementary data to this article can be found online at https://doi.org/10.1016/j.lithos.2024.107783.

References

Ague, J.J., Axler, J.A., 2016. Interface coupled dissolution-reprecipitation in garnet from subducted granulites and ultrahigh-pressure rocks revealed by phosphorous, sodium, and titanium zonation. Am. Mineral. 101, 1696–1699.
Ague, J.J., Baxter, E.F., 2007. Brief thermal pulses during mountain building recorded by Sr diffusion in apatite and multicomponent diffusion in garnet. Earth Planet. Sci. Lett. 261, 500–516.
Ague, J.J., Carlson, W.D., 2013. Metamorphism as garnet sees it: the kinetics of nucleation and growth, equilibration, and diffusional relaxation. Elements 9, 439–445.
Ague, J.J., Eckert Jr., J.O., 2012. Precipitation of rutile and ilmenite needles in garnet: Implications for extreme metamorphic conditions in the Acadian Orogen, USA. Am. Mineral. 97, 840–855.
Ague, J.J., Baxter, E.F., Eckert Jr., J.O., 2001. High fO_2 during sillimanite zone metamorphism of part of the Barrovian type locality, Glen Clova, Scotland. J. Petrol. 42, 1301–1320.
Barrow, G., 1893. On an Intrusion of Muscovite-biotite Gneiss in the South-eastern Highlands of Scotland, and its accompanying Metamorphism. Q. J. Geol. Soc. 49, 330–358.
Baumgartner, L., Floess, D., Podladchikov, Y., Foster Jr., C., 2010. Pressure Gradients in Garnets Induced by Diffusion Relaxation of Major Element Zoning. Geological Society of America, Denver, USA.
Baxter, E.F., Ague, J.J., Depaolo, D.J., 2002. Prograde temperature–time evolution in the Barrovian type–locality constrained by Sm/Nd garnet ages from Glen Clova, Scotland. J. Geol. Soc. 159, 71–82.

Bloch, E.M., Jollands, M.C., Devoir, A., Bouvier, A.S., Ibañez-Mejia, M., Baumgartner, L. P., 2020. Multispecies diffusion of yttrium, rare earth elements and hafnium in garnet. J. Petrol. 61, egaa055.
Blundy, J., Wood, B., 2003. Partitioning of trace elements between crystals and melts. Earth Planet. Sci. Lett. 210, 383–397.
Borinski, S.A., Hoppe, U., Chakraborty, S., Ganguly, J., Bhowmik, S.K., 2012. Multicomponent diffusion in garnets I: general theoretical considerations and experimental data for Fe–Mg systems. Contrib. Mineral. Petrol. 164, 571–586.
Cahn, J.W., Larché, F.C., 1983. An invariant formulation of multicomponent diffusion in crystals. Scr. Metall. 17, 927–932.
Chakraborty, S., Ganguly, J., 1991. Compositional zoning and cation diffusion in garnets. In: Diffusion, Atomic Ordering, and Mass Transport: Selected Topics in Geochemistry, 8. Springer US, New York, NY, pp. 120–175.
Chen, J., Chu, X., 2024. Bridging the gap in garnet diffusion models at low temperatures: Recalibration using Western Tianshan eclogitic breccia. J. Petrol. 65, egae012.
Cheng, H., King, R.L., Nakamura, E., Vervoort, J.D., Zhou, Z., 2008. Coupled Lu–Hf and Sm–Nd geochronology constrains garnet growth in ultra-high-pressure eclogites from the Dabie orogen. J. Metamorph. Geol. 26, 741–758.
Cherniak, D.J., Ryerson, F.J., 1993. A study of strontium diffusion in apatite using Rutherford backscattering spectroscopy and ion implantation. Geochim. Cosmichim. Acta 57, 4653–4662.
Cherniak, D.J., Watson, E.B., 2003. Diffusion in zircon. Rev. Mineral. Geochem. 53, 113–143.
Chu, X., Ague, J.J., 2015. Analysis of experimental data on divalent cation diffusion kinetics in aluminosilicate garnets with application to timescales of peak Barrovian metamorphism, Scotland. Contrib. Mineral. Petrol. 170, 1–27.
Chu, X., Ague, J.J., Podladchikov, Y.Y., Tian, M., 2017. Ultrafast eclogite formation via melting-induced overpressure. Earth Planet. Sci. Lett. 479, 1–7.
Clavijo, S.P., Espath, L., Sarmiento, A., Calo, V.M., 2022. A continuum theory for mineral solid solutions undergoing chemo-mechanical processes. Contin. Mech. Thermodyn. 34, 17–38.
Costa, F., Chakraborty, S., Dohmen, R., 2003. Diffusion coupling between trace and major elements and a model for calculation of magma residence times using plagioclase. Geochim. Cosmochim. Acta 67, 2189–2200.
Cruz-Uribe, A.M., Hoisch, T.D., Wells, M.L., Vervoort, J.D., Mazdab, F.K., 2015. Linking thermodynamic modelling, Lu–Hf geochronology and trace elements in garnet: New P–T–t paths from the Sevier hinterland. J. Metamorph. Geol. 33, 763–781.
Cui, Z., Gao, F., Qu, J., 2012. A finite deformation stress-dependent chemical potential and its applications to lithium ion batteries. J. Mech. Phys. Solids 60, 1280–1295.
Dabrowski, M., Powell, R., Podladchikov, Y., 2015. Viscous relaxation of grain-scale pressure variations. J. Metamorph. Geol. 33, 859–868.
Devoir, A., Bloch, E., Müntener, O., 2021. Residence time of igneous garnet in Si-rich magmatic systems: Insights from diffusion modeling of major and trace elements. Earth Planet. Sci. Lett. 560, 116771.
Dragovic, B., Guevara, V.E., Caddick, M.J., Baxter, E.F., Kylander-Clark, A.R., 2016. A pulse of cryptic granulite-facies metamorphism in the Archean Wyoming Craton revealed by Sm–Nd garnet and U–Pb monazite geochronology. Precambrian Res. 283, 24–49.
Erambert, M., Austrheim, H., 1993. The effect of fluid and deformation on zoning and inclusion patterns in poly-metamorphic garnets. Contrib. Mineral. Petrol. 115, 204–214.
Erba, A., Mahmoud, A.R., Orlando, R., Dovesi, R., 2014. Elastic properties of six silicate garnet end members from accurate ab initio simulations. Phys. Chem. Miner. 41, 151–160.
Erdélyi, Z., Schmitz, G., 2012. Reactive diffusion and stresses in spherical geometry. Acta Mater. 60, 1807–1817.
Faryad, S.W., Chakraborty, S., 2005. Duration of Eo-Alpine metamorphic events obtained from multicomponent diffusion modeling of garnet: a case study from the Eastern Alps. Contrib. Mineral. Petrol. 150, 306–318.
Florence, F.P., Spear, F.S., 1995. Intergranular diffusion kinetics of Fe and Mg during retrograde metamorphism of a pelitic gneiss from the Adirondack Mountains. Earth Planet. Sci. Lett. 134, 329–340.
Gaidies, F., Morneau, Y.E., Petts, D.C., Jackson, S.E., Zagorevski, A., Ryan, J.J., 2021. Major and trace element mapping of garnet: Unravelling the conditions, timing and rates of metamorphism of the Snowcap assemblage, west-Central Yukon. J. Metamorph. Geol. 39, 133–164.
Ganguly, J., 2010. Cation diffusion kinetics in aluminosilicate garnets and geological applications. Rev. Mineral. Geochem. 72, 559–601.
Ganguly, J., Bhattacharya, R.N., Chakraborty, S., 1988. Convolution effect in the determination of composition profiles and diffusion coefficients by microprobe step scans. Am. Mineral. 73, 901–909.
Gorsky, W.S., 1935. Theorie der elastischen Nachwirkung in ungeordneten Mischkristallen (elastische Nachwirkung zweiter Art). Phys. Zeitschrift Sowjetunion 8, 457–471.
Gurtin, M.E., Fried, E., Anand, L., 2010. The Mechanics and Thermodynamics of Continua. Cambridge University Press.
Herring, C., 1950. Diffusional viscosity of a polycrystalline solid. J. Appl. Phys. 21, 437–445.
Hess, B.L., Ague, J.J., 2021. Quantifying the effects of non-hydrostatic stress on single-component polymorphs. J. Geophys. Res. Solid Earth 126, e2020JB021594.
Hess, B.L., Ague, J.J., 2023. Modeling diffusion in ionic, crystalline solids with internal stress gradients. Geochim. Cosmochim. Acta 354, 27–37.
Hess, B.L., Ague, J.J., Voorhees, P.W., 2022. Quantifying the effects of non-hydrostatic stress on multi-component minerals. J. Geophys. Res. Solid Earth 127, e2022JB025201.
Holland, T.J.B., Powell, R., 2011. An improved and extended internally consistent thermodynamic dataset for phases of petrological interest, involving a new equation of state for solids. J. Metamorph. Geol. 29, 333–383.
Karato, S.I., Wang, Z., Liu, B., Fujino, K., 1995. Plastic deformation of garnets: systematics and implications for the rheology of the mantle transition zone. Earth Planet. Sci. Lett. 130, 13–30.
Kohn, M.J., 2014. "Thermoba-Raman-try": Calibration of spectroscopic barometers and thermometers for mineral inclusions. Earth Planet. Sci. Lett. 388, 187–196.
Kohn, M.J., Penniston-Dorland, S.C., 2017. Diffusion: Obstacles and opportunities in petrochronology. Rev. Mineral. Geochem. 83, 103–152.
Kohn, M.J., Spear, F., 2000. Retrograde net transfer reaction insurance for pressure-temperature estimates. Geology 28, 1127–1130.
Larché, F.C., Cahn, J.W., 1982. The effect of self-stress on diffusion in solids. Acta Metall. 30, 1835–1845.
Larché, F.C., Cahn, J.W., 1985. Overview no. 41 the interactions of composition and stress in crystalline solids. Acta Metall. 33, 331–357.
Lasaga, A.C., 1983. Geospeedometry: An extension of geothermometry. In: Kinetics and Equilibrium in Mineral Reactions. Springer New York, New York, NY, pp. 81–114.
McLellan, E., 1985. Metamorphic reactions in the kyanite and sillimanite zones of the Barrovian type area. J. Petrol. 26, 789–818.
Murri, M., et al., 2018. Raman elastic geobarometry for anisotropic mineral inclusions. Am. Mineral. 103, 1869–1872.
Parkinson, C.D., 2000. Coesite inclusions and prograde compositional zonation of garnet in whiteschist of the HP-UHPM Kokchetav massif, Kazakhstan: a record of progressive UHP metamorphism. Lithos 52, 215–233.
Perchuk, A., Philippot, P., Erdmer, P., Fialin, M., 1999. Rates of thermal equilibration at the onset of subduction deduced from diffusion modeling of eclogitic garnets, Yukon-Tanana terrane, Canada. Geology 27, 531–534.
Philpotts, A.R., Ague, J.J., 2022. Principles of Igneous and Metamorphic Petrology. Cambridge University Press.
Powell, R., Evans, K.A., Green, E.C., White, R.W., 2018. On equilibrium in non-hydrostatic metamorphic systems. J. Metamorph. Geol. 36, 419–438.
Putnis, A., Austrheim, H., 2010. Fluid-induced processes: metasomatism and metamorphism. Geofluids 10, 254–269.
Roache, P.J., 1972. Computational Fluid Dynamics. Hermosa Publishers, New Mexico.
Rogowitz, A., Thielmann, M., Kraus, K., Grasemann, B., Renner, J., 2023. The effect of the garnet content on deformation mechanisms and weakening of eclogite: Insights from deformation experiments and numerical simulations. Geochem. Geophys. Geosyst. 24, e2022GC010743.
Ruprecht, P., Plank, T., 2013. Feeding andesitic eruptions with a high-speed connection from the mantle. Nature 500, 68–72.
Scheidl, K.S., Schaeffer, A.K., Petrishcheva, E., Habler, G., Fischer, F.D., Schreuer, J., Abart, R., 2014. Chemically induced fracturing in alkali feldspar. Phys. Chem. Miner. 41, 1–16.
Schwarzenbach, E.M., Zhong, X., Caddick, M.J., Schmalholz, S.M., Menneken, M., Hecht, L., John, T., 2021. On exhumation velocities of high-pressure units based on insights from chemical zoning in garnet (Tianshan, NW China). Earth Planet. Sci. Lett. 570, 117065.
Shi, S., Markmann, J., Weissmüller, J., 2018. Verifying Larché–Cahn elasticity, a milestone of 20th-century thermodynamics. Proc. Natl. Acad. Sci. 115, 10914–10919.
Smye, A., Seman, S., Hudak, M., Crispin, K., 2017. Rates of mantle cooling and exhumation during rifting constrained by REE-in-pyroxene speedometry. Geochem. Geophys. Geosyst. 18, 2510–2525.
Spear, F.S., 1991. On the interpretation of peak metamorphic temperatures in light of garnet diffusion during cooling. J. Metamorph. Geol. 9, 379–388.
Spear, F.S., Ashley, K.T., Webb, L.E., Thomas, J.B., 2012. Ti diffusion in quartz inclusions: implications for metamorphic time scales. Contrib. Mineral. Petrol. 164, 977–986.
Stephenson, G.B., 1988. Deformation during interdiffusion. Acta Metall. 36, 2663–2683.
Tajčmanová, L., Podladchikov, Y., Powell, R., Moulas, E., Vrijmoed, J.C., Connolly, J.A. D., 2014. Grain-scale pressure variations and chemical equilibrium in high-grade metamorphic rocks. J. Metamorph. Geol. 32, 195–207.
Tajčmanová, L., Vrijmoed, J., Moulas, E., 2015. Grain-scale pressure variations in metamorphic rocks: implications for the interpretation of petrographic observations. Lithos 216, 338–351.
Tajčmanová, L., Podladchikov, Y., Moulas, E., Khakimova, L., 2021. The choice of a thermodynamic formulation dramatically affects modelled chemical zoning in minerals. Sci. Rep. 11, 18740.
Tomozawa, M., Davis, K.M., 1999. Time dependent diffusion coefficient of water into silica glass at low temperatures. Mater. Sci. Eng. A 272, 114–119.
Van Orman, J.A., Grove, T.L., Shimizu, N., 2001. Rare earth element diffusion in diopside: influence of temperature, pressure, and ionic radius, and an elastic model for diffusion in silicates. Contrib. Mineral. Petrol. 141, 687–703.
Viete, D.R., Lister, G.S., 2017. On the significance of short-duration regional metamorphism. J. Geol. Soc. Lond. 174, 377–392.
Voorhees, P.W., Johnson, W.C., 2004. The thermodynamics of elastically stressed crystals. In: Ehrenreich, H., Spaepen, F. (Eds.), Solid State Physics. Elsevier, pp. 1–201, 59 pp.

Vorhies, S.H., Ague, J.J., 2011. Pressure–temperature evolution and thermal regimes in the Barrovian zones, Scotland. J. Geol. Soc. Lond. 168, 1147–1166.
Wang, Z., Ji, S., 1999. Deformation of silicate garnets: Brittle-ductile transition and its geological implications. Can. Mineral. 37, 525–541.
Watson, E.B., Baxter, E.F., 2007. Diffusion in solid-Earth systems. Earth Planet. Sci. Lett. 253, 307–327.
Wheeler, J., 2018. The effects of stress on reactions in the Earth: sometimes rather mean, usually normal, always important. J. Metamorph. Geol. 36, 439–461.
White, R.W., Powell, R., Johnson, T.E., 2014. The effect of Mn on mineral stability in metapelites revisited: New a–x relations for manganese-bearing minerals. J. Metamorph. Geol. 32, 809–828.
Yamato, P., Duretz, T., Angiboust, S., 2019. Brittle/ductile deformation of eclogites: insights from numerical models. Geochem. Geophys. Geosyst. 20, 3116–3133.
Zener, C., 1948. Theory of strain interaction of solute atoms. Phys. Rev. 74, 639–647.
Zhong, X., Vrijmoed, J., Moulas, E., Tajčmanová, L., 2017. A coupled model for intragranular deformation and chemical diffusion. Earth Planet. Sci. Lett. 474, 387–396.
Zhong, X., Andersen, N.H., Dabrowski, M., Jamtveit, B., 2019. Zircon and quartz inclusions in garnet used for complementary Raman thermobarometry: application to the Holsnøy eclogite, Bergen Arcs, Western Norway. Contrib. Mineral. Petrol. 174, 1–17.